SIAM J. IMAGING SCIENCES
Vol. 6, pp. 1

616–659

Uniqueness and Approximation of a Photometric Shape-from-Shading Model*

Roberto Mecca† and Maurizio Falcone†

Abstract. We deal with an inverse problem where we want to determine the surface of an object using the information contained in two or more pictures which correspond to different light conditions. In particular, we will examine the case where the light source direction varies between the pictures, and we will show how this additional information allows us to obtain a uniqueness result solving the well-known convex/concave ambiguity of the shape-from-shading problem. We will prove a uniqueness result for weak (Lipschitz continuous) solutions that improves previous results in [R. Kozera, *Appl. Math. Comput.*, 44 (1991), pp. 1–103] and [R. Onn and A. Bruckstein, *Int. J. Comput. Vision*, 5 (1990), pp. 105–113]. We also propose some approximation schemes for the numerical solution of this problem and analyze the properties of two approximation schemes: an upwind finite difference scheme and a semi-Lagrangian scheme. Finally, we present some numerical tests on smooth and nonsmooth surfaces coming from virtual and real images.

Key words. shape-from-shading, photometric stereo, nonlinear systems, Hamilton–Jacobi equations, semi-Lagrangian schemes, implicit upwind finite difference scheme

AMS subject classifications. 68T45, 35A02, 65N21, 65N12, 65M25

DOI. 10.1137/110857258

1. Introduction.

The three-dimensional (3D) reconstruction of an object is a classical problem in computer vision which has always attracted a great deal of attention, starting from the pioneering works of Horn and Brooks; see, e.g., their book [20]. This is a difficult inverse problem where the goal is to reconstruct the surface from a single image; moreover, it is now well known that this problem is ill-posed since there can be many solutions (no matter which regularity is required for the solutions) unless additional conditions/information is added to the problem [49, 12]. This explains the growing importance of a generalization of this classical problem which can take into account multiple images of the same object. These images should contain more information on the object as is the case for images taken from different points under the same light conditions (stereovision) or from the same point under different light conditions (photometric stereo). Our paper is devoted to the analysis and approximation of the photometric stereo problem via a partial differential equation (PDE) model for which we will prove uniqueness.

From the point of view of applications, the shape-from-shading photometric stereo (SfS-PS) problem has a great potential impact since laser scanners are rather expensive and can produce a 3D reconstruction only for objects with small dimensions since they must fit into the detector. Moreover, the distance from the object may represent a problem in the use of laser

*Received by the editors November 29, 2011; accepted for publication (in revised form) September 21, 2012; published electronically March 21, 2013. This work was partially supported by the PRIN 2009 Project "Modelli numerici per il calcolo scientifico ed applicazioni avanzate."
http://www.siam.org/journals/siims/6-1/85725.html
†Dipartimento di Matematica, SAPIENZA - Università di Roma, 00185 Rome, Italy (mecca.roberto@gmail.com, falcone@mat.uniroma1.it).

scanners. These physical difficulties have reduced the impact of the 3D scanner technology in many areas, so that the preservation of sculptures and other artifacts in digital archives is still limited.

In order to overcome these difficulties, several researchers have proposed using one or more digital pictures of the object as basic data for the 3D reconstruction, that is, the SfS problem [20, 12, 19]. Even if the first to take an interest in the problem were some opticians [8, 16, 39], the rise of the computer age has marked a true turning point in research in this area, driven by the efforts of Horn [20, 18] and his collaborators at MIT. All of these activities were devoted to solving the inverse problem in the framework of smooth solutions. More recently, starting from the first work of Lions (see [40, 26]) new results have been obtained in the framework of weak solutions (in the viscosity sense), giving SfS problems a stronger theoretical foundation.

To put this paper into perspective, let us refer to previous works on SfS and SfS-PS. Many papers have been written to obtain the surface only using a single picture, and it is well known that the problem is ill-posed (see the surveys by Zhang et al. [49] and by Durou, Falcone, and Sagona [12]). In fact it has been shown that there is no uniqueness even for regular solutions due to the convex/concave ambiguity. Because of that it was natural to introduce new models where one can use more than one picture. An interesting result has been obtained by Chambolle [5] considering the *stereo vision technique*: he proved that if we have two images of the same object taken from two different points of view (*with the same light source*), then the solution of the problem is unique. Other tentatives have been made to set up a well-posed problem and overcome some limitations of the model. A number of papers deal with the perspective SfS model [35, 45, 7, 3], and it has been proved that for I continuous there is a unique solution in the viscosity sense, provided that one can apply a "neutral" set of boundary conditions (usually referred to as state constrained boundary conditions in the literature); these boundary conditions are very natural if the model has an attenuation term depending on the distance between the object and the camera. However, it has been shown that even the perspective SfS model suffers in general for the presence of ambiguities when the brightness function is not regular I (see the recent paper [4] for more details).

In the framework of photometric stereo models, the perspective formulation of the SfS problem has been considered only by [44]. In that paper the authors study the problem exploiting three perspective images without adopting the most used variables $p = u_x$ and $q = u_y$. In this approach they do not solve the PDE problem but compute the height u of the surface by the classical technique of integration along paths (see [48, 10, 11] for more details).

The technique that we will analyze here is the SfS-PS, where we have as inputs several images of the object (always photographed from the same point of view) and the corresponding light source position for each image. This problem was originally introduced by Onn and Bruckstein [31] and Kozera [22].

The first step is to construct a formulation of the problem that allows us to obtain the uniqueness of solution, and that is coherent with the single image model. We will see how this formulation is also efficient from the computational point of view. The analysis of this differential approach has given other interesting results on the SfS-PS problem such as those contained in the papers [27] and [28], where several features such as uniqueness of normal vectors and symmetries of surface are exploited.

The outline of the paper is the following.

In section 2 we introduce our hypotheses and describe the classical SfS orthographic problem where only one image is used. In section 3 the new differential approach is explained in detail, also giving some results used to prove the uniqueness of the weak solution. This proof will be the main result of section 4, which also contains the setting of boundary conditions in order to have a well-posed differential problem. Section 5 is devoted to the analysis of two approximation schemes: the first is an upwind finite difference scheme, whereas the second is a semi-Lagrangian scheme. We will prove some properties for these schemes, and, in particular, we will establish convergence for both of them. Finally, we will present a number of numerical results using the above-mentioned schemes. We have taken into account virtual and real images, also considering smooth and nonsmooth solutions.

2. Shape from shading and photometric stereo technique. We start by giving an outline of the SfS problem and introducing our basic assumptions. In this paper we work on the simplest version of the SfS problem, where we attach the camera to a 3D coordinate system $(Oxyz)$ such that Oxy coincides with the image plane and Oz coincides with the optical axis. The classical assumptions for this model are the following:

(A1) The light sources are at infinity.
(A2) The surface is Lambertian.
(A3) There are no self-reflections on the surface.
(A4) There are no black shadows on the surface.
(A5) The optical point is sufficiently far from the surface so that perspective deformations can be neglected.

We will assume that there is a unique light source at infinity whose direction is indicated by the unit vector $\omega = (\omega_1, \omega_2, \omega_3) = (\widetilde{\omega}, \omega_3) \in \mathbb{R}^3$, where $(\omega_3 > 0)$. The assumption on the complete illumination of the surface from the light source ω is guaranteed by the following condition:

$$u((x,y) + t\widetilde{\omega}) < u(x,y) + t\omega_3 \quad \forall t > 0. \tag{2.1}$$

Under the assumption of orthographic projection, the visible part of the scene is, up to a scale factor, a graph $z = u(x,y)$, where (x,y) is an image point. It is well known [20] that the SfS problem can be modeled by the *image irradiance equation*:

$$R(n(x,y)) = I(x,y), \tag{2.2}$$

where $I(x,y)$ is the gray level measured in the image at (x,y) (in fact $I(x,y)$ is the irradiance at (x,y), but both quantities are proportional) and $R(n(x,y))$ is the reflectance function, giving the value of the light re-emitted by the surface as a function of its orientation (i.e., of the unit normal $n(x,y)$ to the surface at point $(x,y,u(x,y))$. This normal can easily be expressed as

$$n(x,y) = \frac{1}{\sqrt{1 + |\nabla u(x,y)|^2}}(-\nabla u(x,y), 1), \tag{2.3}$$

where $\nabla u(x,y) = (\frac{\partial u}{\partial x}(x,y), \frac{\partial u}{\partial y}(x,y))$. Irradiance function I is the datum in the model since it is measured at each pixel of the image, for example, in terms of a gray level (from 0 to

255). In order to construct a continuous model, we will assume that I takes real values in the interval $[0,1]$. The function $u:\overline{\Omega}\to\mathbb{R}$ representing the height of the surface at every point (which is the unknown of our problem) has to be reconstructed on a compact domain $\overline{\Omega}\subset\mathbb{R}^2$ (the *reconstruction domain*). Also assume for simplicity that ω is given (in some works, ω as well is considered as unknown (see [6, 9]) even if this problem is sometimes ill-posed [2]). In our case

$$R(n(x,y)) = \rho(x,y)(\omega\cdot n(x,y)),$$

and, considering a Lambertian surface of uniform albedo $\rho(x,y)\equiv 1$, (2.2) can be written using (2.3):

$$I(x,y)\sqrt{1+|\nabla u(x,y)|^2}+\widetilde{\omega}\cdot\nabla u(x,y)-\omega_3=0 \quad \forall (x,y)\in\Omega, \tag{2.4}$$

which is a first order nonlinear PDE of Hamilton–Jacobi type. Note that the equation depends only on ∇u, so if u is a solution, $u+constant$ is also a solution. In order to have a well-posed problem we must add the Dirichlet boundary condition $u(x,y)=g(x,y)$ for all $(x,y)\in\partial\Omega$, which we will assume given in our problem (and this is a nontrivial assumption). Then the complete problem can be written as follows:

$$\begin{cases} H(x,y,\nabla u(x,y))=0 & \text{on } \Omega,\\ u(x,y)=g(x,y) & \text{on } \partial\Omega, \end{cases} \tag{2.5}$$

where H is the Hamiltonian of the problem.

Points $(x,y)\in\Omega$ such that $I(x,y)$ is maximal correspond to the particular situation where ω and $n(x,y)$ have the same direction: these points are usually called *singular points*.

Let us mention that (2.4) is not the most general equation of SfS [32]: since real surfaces are not purely Lambertian, some papers are concerned with non-Lambertian SfS problems [1, 24, 38]; moreover, the situation is more complex in the presence of other lighting models [42, 47] or when the interreflections are taken into account [29, 15]. We will also consider the equation which appears in most of the papers and corresponds to a frontal light source at infinity (i.e., $\omega=(0,0,1)$). Then (2.4) becomes the "eikonal equation":

$$|\nabla u(x,y)| = f(x,y), \quad (x,y)\in\Omega, \tag{2.6}$$

where

$$f(x,y)=\sqrt{\frac{1}{I(x,y)^2}-1}. \tag{2.7}$$

In the last few years, new models have appeared. The main goal of those models is to modify the classical assumptions in order to deal with real-life applications. The major modification that has been considered is to replace the usual assumption that the projection of scene points during a photographic process is orthographic with the more realistic assumption of perspective projection [33, 23, 17, 30, 41, 34, 45]. Even if this evolution of the orthographic problem is a concrete step forward for the SfS problem, all the cited works do not allow one to obtain a unique solution when considering as given data a single (perspective) image and the direction of the respective light source.

We want to emphasize one more time that using only one image, because of the presence of singular points, it is not possible to find the unique solution of the SfS problems. This is also true for some perspective SfS problems. In fact, even for more complicated perspective models [35], where the light source is taken close to the object, it is not possible to obtain uniqueness [3]. To try to find the unique solution, we increase the information about the surface in a natural way (i.e., starting with the same data types of the SfS problem). The technique we use to increase the information in this sense is the photometric stereo (SfS-PS) method.

Let us assume that we have k different pictures of the same surface taken from the same point of view but using a different light source for each image. This will produce k equations similar to (2.4), i.e.,

$$I_i(x,y) = n(x,y)\cdot\omega^i \quad \forall (x,y)\in\Omega,\ i=1,\dots,k. \tag{2.8}$$

3. Photometric stereo: A review of previous results. There are various possible approaches to constructing a model for the SfS-PS problem even in the simple case of a graph surface. In this work we will focus our attention on a model where the unknown is given by the height of the surface, studying the conditions which can guarantee a uniqueness result (giving a complete characterization of the solution) and developing a numerical method for the approximation of u.

Let us introduce the SfS-PS problem for two directions of the light sources (ω' and ω''). Following Kozera [22], we obtain the system of nonlinear PDEs

$$\begin{cases} \dfrac{-\nabla u(x,y)\cdot\widetilde{\omega}'+\omega_3'}{\sqrt{1+|\nabla u(x,y)|^2}} = I_1(x,y) & \forall (x,y)\in\Omega, \\ \dfrac{-\nabla u(x,y)\cdot\widetilde{\omega}''+\omega_3''}{\sqrt{1+|\nabla u(x,y)|^2}} = I_2(x,y) & \forall (x,y)\in\Omega, \end{cases} \tag{3.1}$$

coupled with the Dirichlet boundary condition $u(x,y)=g(x,y)$, which we assume to be given for every $(x,y)\in\partial\Omega$.

For the reader's convenience we briefly recall the uniqueness results for regular solutions proved by Kozera [22]. The starting point is the following technical lemma.

Lemma 3.1. *At every point $(x,y)\in\Omega$ the first derivatives of u can be expressed in terms of I_1, I_2, ω', and ω'' in the following form (we have omitted the dependence on (x,y) of $u_x^{\pm}$, I_1, I_2, and Λ):*

$$u_x^{\pm} = \frac{(\omega_1''(\omega'\cdot\omega'')-\omega_1')I_1+(\omega_1'(\omega'\cdot\omega'')-\omega_1'')I_2 \pm (\omega_3'\omega_2''-\omega_2'\omega_3'')\varepsilon\sqrt{\Lambda}}{(\omega_3'-\omega_3''(\omega'\cdot\omega''))I_1+(\omega_3''-\omega_3'(\omega'\cdot\omega''))I_2 \pm (\omega_1'\omega_2''-\omega_2'\omega_1'')\varepsilon\sqrt{\Lambda}}, \tag{3.2}$$

$$u_y^{\pm} = \frac{(\omega_2''(\omega'\cdot\omega'')-\omega_2')I_1+(\omega_2'(\omega'\cdot\omega'')-\omega_2'')I_2 \pm (\omega_1'\omega_3''-\omega_3'\omega_1'')\varepsilon\sqrt{\Lambda}}{(\omega_3'-\omega_3''(\omega'\cdot\omega''))I_1+(\omega_3''-\omega_3'(\omega'\cdot\omega''))I_2 \pm (\omega_1'\omega_2''-\omega_2'\omega_1'')\varepsilon\sqrt{\Lambda}}, \tag{3.3}$$

where

$$\Lambda = \Lambda(x,y) := 1 - I_1^2(x,y) - I_2^2(x,y) - (\omega'\cdot\omega'')[\omega'\cdot\omega'' - 2I_1(x,y)I_2(x,y)] \tag{3.4}$$

and the function $\varepsilon = \varepsilon(x,y)$ *can take only the values* ± 1 *in such a way that* $f(x,y) = \varepsilon(x,y)\sqrt{\Lambda(x,y)}$ *is continuous.*

Note that by the previous lemma one has two different values for u_x and u_y at every point.

Theorem 3.2. *Let* Ω *be a simply connected region of* $\mathbb{R}^2$*, let* $I_i \in C^1 : \Omega \to [0,1]$*,* $i = 1,2$*, and let* I_1*,* $I_2 \in C^1(\Omega)$*. Suppose that* $\Lambda > 0$ *on* Ω *and that for each choice of the* $\pm$ *sign,*

$$\sigma^{\pm} = (\omega_3' - \omega_3''(\omega' \cdot \omega''))I_1 + (\omega_3'' - \omega_3'(\omega' \cdot \omega''))I_2 \pm (\omega_1'\omega_2'' - \omega_2'\omega_1'')\sqrt{\Lambda} \tag{3.5}$$

does not vanish over Ω*. Then a necessary and sufficient condition for the existence of exactly two solutions to* (3.1) *of class* C^2 *is*

$$\frac{\partial}{\partial y}u_x^+(x,y) = \frac{\partial}{\partial x}u_y^+(x,y) \text{ or } \frac{\partial}{\partial y}u_x^-(x,y) = \frac{\partial}{\partial x}u_y^-(x,y) \tag{3.6}$$

with $u_x^{\pm}$ *and* $u_y^{\pm}$ *defined, respectively, by* (3.2) *and* (3.3)*.*

Corollary 3.3. *Let* Ω *be a simply connected region of* $\mathbb{R}^2$*, let* $I_i \in C^1 : \Omega \to [0,1]$*,* $i = 1,2$*, and let* I_1*,* $I_2 \in C^1(\Omega)$*. Suppose that* $\Lambda \equiv 0$ *on* Ω *and that*

$$\sigma = (\omega_3' - \omega_3''(\omega' \cdot \omega''))I_1 + (\omega_3'' - \omega_3'(\omega' \cdot \omega''))I_2 \tag{3.7}$$

does not vanish over Ω*. Then, a necessary and sufficient condition for the existence of exactly one solution* $u \in C^2(\Omega)$ *to* (3.1) *is*

$$\frac{\partial}{\partial y}u_x(x,y) = \frac{\partial}{\partial x}u_y(x,y) \tag{3.8}$$

with u_x *and* u_y *defined, respectively, in* (3.2) *and* (3.3) *taken with* $\Lambda \equiv 0$*.*

Using the analysis given in [27] it is possible to show that the set of points for which $D_0 := \{(x,y) \in \Omega : \Lambda(x,y) = 0\}$ is not the only one that allows us to obtain uniqueness of the first partial derivative. In fact there exists another set D_1 in the image domain Ω where there are no ambiguities on the first derivative, since one of the two normals to the surface has no physical meaning. It should be noted that these sets are not easy to find because they strongly depend on the position of the light sources and on the surface. However, the measure of these sets is usually very small with respect to the image domain Ω (typically D_0 has measure 0).

Let us also mention that the hypotheses of regularity on the data (e.g., I_1, $I_2 \in C^1(\Omega)$) is not a sufficient condition for the uniqueness of u even in the regular case because of the strong hypothesis $\Lambda \equiv 0$ in Ω.

As we said in the introduction, we want to focus our attention on the regularity of u reducing the hypotheses and allowing for weaker solutions, e.g., Lipschitz continuous solutions.

In general, two cases must be considered in the analysis of this problem:

(C1) the *nonphysical case*, where we wonder whether there exists a surface u related to the images I_1, I_2 and to a couple of vectors ω' and ω'' which are *not correlated* (i.e., the images I_1, I_2 do not correspond to the light sources at ω' and ω'');

(C2) the *physical case*, where we assume the existence of a surface u and the two images I_1 and I_2 are correlated since they are expressed in terms of ω' and ω'' as

$$I_1(x,y) = \frac{-\nabla u(x,y) \cdot \widetilde{\omega}' + \omega_3'}{\sqrt{1 + |\nabla u(x,y)|^2}}, \quad I_2(x,y) = \frac{-\nabla u(x,y) \cdot \widetilde{\omega}'' + \omega_3''}{\sqrt{1 + |\nabla u(x,y)|^2}}. \tag{3.9}$$

In what follows we will focus our attention on the physical case (C2) which is clearly more interesting for computer vision applications.

4. A new differential approach to the SfS-PS using two images. Let us start with a simple 1-*D case* (where $\overline{\Omega} = [a, b]$ and $\omega' = (\omega_1', \omega_2')$, $\omega'' = (\omega_1'', \omega_2'')$) to fix some ideas of our method. The SfS problem leads to the following nonlinear system of PDEs:

$$\begin{cases} \dfrac{-u_x(x)\omega_1' + \omega_2'}{\sqrt{1+u_x(x)^2}} = I_1(x) & \text{a.e. } x \in \Omega, \\ \dfrac{-u_x(x)\omega_1'' + \omega_2''}{\sqrt{1+u_x(x)^2}} = I_2(x) & \text{a.e. } x \in \Omega, \\ u(a) = u_a, u(b) = u_b & \text{with } u_a, u_b \in \mathbb{R}. \end{cases} \tag{4.1}$$

Note that the PDEs appearing in the SfS-PS model are all of first order. Setting the equation a.e., we allow for solutions which are differentiable a.e. in Ω, so we allow for Lipschitz continuous solutions due to the Rademacher theorem [37].

For the nonlinear system (4.1) the next result stands.

Theorem 4.1. *Let ω' and ω'' be two linearly independent vectors. Let $I_1(x)$, $I_2(x) \in L^\infty(\Omega)$ such that $0 < I_1(x), I_2(x) \leq 1$ for $x \in \overline{\Omega}$, where Ω is a connected subset of $\mathbb{R}$. Then, there exists a unique Lipschitz continuous solution $u(x)$ for the system (4.1) determined from a single boundary condition.*

Proof. If we consider

$$\nu_1 = -\frac{u_x}{\sqrt{1+u_x^2}} \quad \text{and} \quad \nu_2 = \frac{1}{\sqrt{1+u_x^2}}, \tag{4.2}$$

then it is possible to rewrite the system (4.1) as

$$\begin{pmatrix} \omega_1' & \omega_2' \\ \omega_1'' & \omega_2'' \end{pmatrix} \begin{pmatrix} \nu_1 \\ \nu_2 \end{pmatrix} = \begin{pmatrix} I_1 \\ I_2 \end{pmatrix}. \tag{4.3}$$

If the light source vectors are linearly independent, the linear algebraic system (4.3) has a unique solution (ν_1, ν_2). From ν we can easily get u_x, in fact, $u_x = -\frac{\nu_1}{\nu_2}$. If we know the first derivative, we can compute u from the fundamental theorem of calculus:

$$u(x) = u_a + \int_a^x u_x(s)ds \tag{4.4}$$

or, starting from b,

$$u(x) = u_b - \int_x^b u_x(s)ds. \tag{4.5}$$

Note that the use of boundary conditions is crucial in obtaining u by integration. ∎

Note that if we repeat the same argument in dimension n considering $n+1$ light sources, it is always possible to write a formula for the first partial derivatives of a smooth surface as shown in [22]. Clearly one of the troubles in this problem is to reduce as much as possible

the number of light sources (i.e., the number of images) necessary to get a single surface. The next step will be to consider the *two-dimensional* (2D) *case* repeating the elimination of the nonlinearity. We try to reduce the space dimension of the problem by looking for a solution with only two images corresponding to two (known) light sources.

Let us consider the system (3.1) and eliminate the nonlinearity in the first equation by the relation

$$\sqrt{1+|\nabla u(x,y)|^2} = \frac{-\nabla u(x,y)\cdot\widetilde{\omega}' + \omega_3'}{I_1(x,y)}. \tag{4.6}$$

Substituting it into the second equation we obtain the following linear equation:

$$\begin{aligned}(I_2(x,y)\omega_1' - I_1(x,y)\omega_1'')\frac{\partial u}{\partial x} &+ (I_2(x,y)\omega_2' - I_1(x,y)\omega_2'')\frac{\partial u}{\partial y}\\ &= (I_2(x,y)\omega_3' - I_1(x,y)\omega_3'') \quad \forall (x,y)\in\Omega.\end{aligned} \tag{4.7}$$

Then adding the Dirichlet boundary condition we obtain

$$\begin{cases} b(x,y)\cdot\nabla u(x,y) = f(x,y) & \forall (x,y)\in\Omega,\\ u(x,y) = g(x,y) & \forall (x,y)\in\partial\Omega, \end{cases} \tag{4.8}$$

where b is a 2D vector field defined in $\overline{\Omega}$ by

$$b(x,y) := (I_2(x,y)\omega_1' - I_1(x,y)\omega_1'', I_2(x,y)\omega_2' - I_1(x,y)\omega_2'') \tag{4.9}$$

and

$$f(x,y) := I_2(x,y)\omega_3' - I_1(x,y)\omega_3''. \tag{4.10}$$

Note that the fact that $b(x,y)$ does not vanish in Ω implies that there are no equilibrium points for the dynamics, so b has neither pits nor source points in the domain. We will see in section 5 a better result that allows us to have a weaker solution using some regularity features of $b(x,y)$.

Solving (4.7) along the characteristic curves (i.e., the trajectories solving the system

$$\begin{cases} \dot{x}(t) = b_1(x,y),\\ \dot{y}(t) = b_2(x,y) \end{cases} \tag{4.11}$$

for any given initial condition), we pass from a 2D PDE to a 1D differential problem. In the general case, the characteristics of the linear differential equation (4.7) will depend on the surface since b depends on I_1 and I_2. This implies that the characteristic curves can have rather complicated shapes, but we need only have b Lipschitz continuous in order to have uniqueness of the characteristics. However, in some particular cases the characteristic curves are very simple and can even be completely independent from the surface $u(x,y)$. This is the case, for example, when the light sources are such that the characteristics are straight lines.

Remark: A variable albedo model. It is interesting to note that in this simple model one can include a variable albedo since this does not affect the solution of our system. The albedo

function ρ has the bounds $0 < \rho(x,y) \leq 1$; since it represents the percentage of light reflected by the object at a point $(x,y) \in \overline{\Omega}$, ρ does not depend on the light sources. Then, considering the photometric stereo equations with the unknown albedo, we get

$$\begin{cases} \rho(x,y)\dfrac{-\nabla u(x,y)\cdot\widetilde{\omega}' + \omega_3'}{\sqrt{1+|\nabla u(x,y)|^2}} = I_1(x,y) & \forall (x,y)\in\Omega, \\ \rho(x,y)\dfrac{-\nabla u(x,y)\cdot\widetilde{\omega}'' + \omega_3''}{\sqrt{1+|\nabla u(x,y)|^2}} = I_2(x,y) & \forall (x,y)\in\Omega. \end{cases} \tag{4.12}$$

Repeating the same arguments as before for the cancellation of the nonlinearity, we can also drop ρ from the final equation (4.7). So, the solution can be reconstructed independently on ρ. Once we have $u(x,y)$ we can easily derive $n(x,y)$, and then we can compute the albedo by applying either of the two irradiance equations, that is,

$$\rho(x,y) = \frac{I_1(x,y)}{\omega'\cdot n(x,y)} \quad \text{or} \quad \rho(x,y) = \frac{I_2(x,y)}{\omega''\cdot n(x,y)}. \tag{4.13}$$

Example 1. We now consider a particular position of the light sources. Let us take the two light vectors $\omega' = (0,0,1)$ and $\omega'' = (\sin(\varphi), 0, \cos(\varphi))$ ($\varphi \in (-\frac{\pi}{2}, 0)\cup(0, \frac{\pi}{2})$); see Figure 1(left). The irradiance equation becomes

$$-I_1(x,y)\sin(\varphi)\frac{\partial u}{\partial x} = (I_2(x,y) - I_1(x,y)\cos(\varphi)) \quad \forall (x,y)\in\Omega. \tag{4.14}$$

This case has been already studied by Lee and Brady [25], who did not generalize the reasoning for all the other possible light source directions. Furthermore it is useful to understand how the information on the surface is given by the light. We can see that the main information is given in the direction of the vector $\widetilde{\omega}''$, which in our case coincides with the direction of the x axis (the same thing, but with the y axis, happens if we take the second light source $\omega'' = (0, \sin(\varphi), \cos(\varphi))$). This allows us to approach a 2D problem like a 1D case, considering it along the characteristic curves.

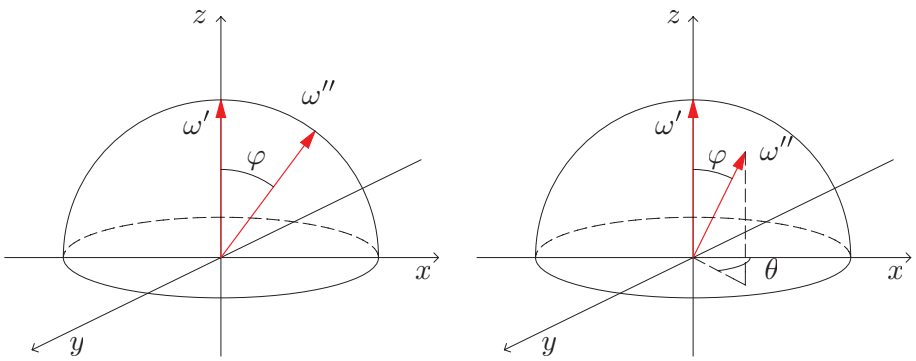

Figure 1. *On the left, the two light sources of Example 1 (that is, coplanar to the xz plane), and on the right, the light vectors of Example 2.*

Example 2. Generalizing the first example, we take the second light as a generic unitary vector (i.e., $\omega'' = (\sin(\varphi)\cos(\theta), \sin(\theta)\sin(\varphi), \cos(\varphi))$ with $\varphi \in (-\frac{\pi}{2}, 0) \cup (0, \frac{\pi}{2})$ and $\theta \in [0, 2\pi]$); see Figure 1(right). We note that the equation becomes

$$-I_1(x,y)\omega_1'' \frac{\partial u}{\partial x} - I_1(x,y)\omega_2'' \frac{\partial u}{\partial y} = I_2(x,y) - I_1(x,y)\omega_3'' \quad \forall (x,y) \in \Omega, \tag{4.15}$$

and the curves where the information is driven by the characteristics are the same as before, that is, still straight lines. In particular, now they are parallel lines with a θ inclination. The approximation of the linear equation (4.7) is, in fact, very difficult if we don't consider schemes that take care of the direction of the luminous information.

5. Existence and uniqueness of the weak solution. In this section we will weaken our assumptions on the solution of (4.8) and ask for solutions which satisfy the equations a.e. $(x, y) \in \Omega$. Since a Lipschitz continuous solution has a gradient a.e. (by the Rademacher theorem [37]), the space of Lipschitz functions in Ω will be a natural choice (this space will be denoted by $\mathrm{Lip}(\Omega)$). We have to complete the analysis extending the uniqueness results from $C^1(\Omega)$ to $\mathrm{Lip}(\Omega)$. This extension will be very useful for real applications since the objects have, in general, nonregular surfaces.

Let us observe that the SfS problem, using only one image, is an ill-posed problem (even for smooth surfaces) due to the convex/concave ambiguity [12, 26].

If we remain in the context of the applications, it is possible to consider the advantage of the study of an inverse problem such as the SfS. In this case (that is, the physical case), in fact, we can understand what happens to the function coefficients $b(x, y)$ and $f(x, y)$. If we consider a solution $u \in \mathrm{Lip}(\Omega)$ and consider the points where it is not differentiable as the family of regular curves $(\gamma_1(t), \ldots, \gamma_k(t))$, where t is the argument of the parametric representation, it is clear that these curves also contain the points of discontinuity of the functions $b(x, y)$ and $f(x, y)$ because they depend on $I_1(x, y)$ and $I_2(x, y)$ by definition. This means that our problem (4.8) has, in the linear equation, discontinuous coefficients. That is, if we consider our differential problem as an inverse problem of SfS with photometric stereo technique, searching for a weak solution implies a study of the linear PDE with discontinuous coefficients. Moreover, there is a relation between the set of points of discontinuity of $b(x, y)$ and $f(x, y)$ and the set of points where the solution u is not differentiable; in fact, they are the same (see Figure 2). Another feature of the discontinuities $b(x, y)$ and $f(x, y)$ comes from the fact that, considering Lipschitz continuous solutions, they can have only jump discontinuities.

Lemma 5.1. *Let us assume to be in the physical case* (C2)*, and let* $(\gamma_1(t), \ldots, \gamma_k(t))$ *be the family of jump discontinuity curves for* b *(i.e., for* I_1 *and* I_2*). Then, the vector field* $b(x, y)$ *does not vanish in* $\overline{\Omega}$*; that is,*

$$|b(x,y)| \neq 0 \quad \forall (x,y) \in \overline{\Omega}. \tag{5.1}$$

Proof. Let us suppose by contradiction that there exists a point $(\overline{x}, \overline{y}) \in \overline{\Omega}$ such that $b(\overline{x}, \overline{y}) = 0$; that is,

$$\begin{cases} I_2(\overline{x},\overline{y})\omega_1' - I_1(\overline{x},\overline{y})\omega_1'' = 0, \\ I_2(\overline{x},\overline{y})\omega_2' - I_1(\overline{x},\overline{y})\omega_2'' = 0. \end{cases} \tag{5.2}$$

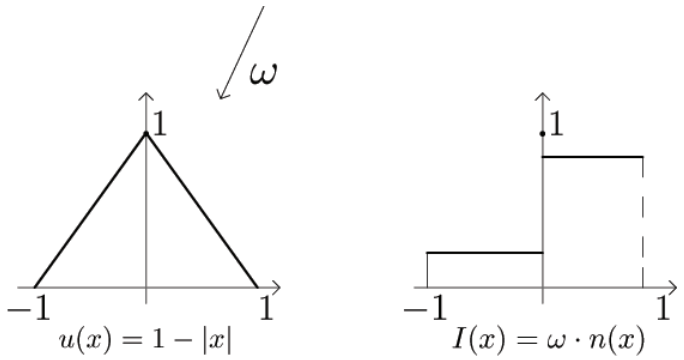

Figure 2. *A schematic example shows that the points where the image function I is discontinuous are the same points for which the solution u is not differentiable. On the left the Lipschitz function; on the right the associated image through the light ω.*

We emphasize that if the point $(\overline{x}, \overline{y})$ belongs to a curve of discontinuity $\gamma_1(t), \ldots, \gamma_k(t)$, the same reasoning holds. It is enough to consider the values $I_1(\overline{x}, \overline{y})$ and $I_2(\overline{x}, \overline{y})$ obtained by the same limit to $(\overline{x}, \overline{y})$.

Now, if $\widetilde{\omega}' = \widetilde{\omega}''$, then also $\omega_3' = \omega_3''$ because the light source directions belong to the upper semisphere. This is redundant with the conclusion of (5.2) (that is, $I_1(x, y) = I_2(x, y)$) since

$$\begin{cases} I_2(x,y)\omega_1 = I_1(x,y)\omega_1, \\ I_2(x,y)\omega_2 = I_1(x,y)\omega_2, \end{cases}$$

where $(\omega_1, \omega_2) = \widetilde{\omega}' = \widetilde{\omega}''$, but it is not the situation of the photometric stereo technique. In this case it is necessary to consider only the case when $\widetilde{\omega}' \neq \widetilde{\omega}''$, that is,

$$\begin{cases} (I_1(\overline{x}, \overline{y}), -I_2(\overline{x}, \overline{y})) \cdot (\omega_1'', \omega_1') = 0, \\ (I_1(\overline{x}, \overline{y}), -I_2(\overline{x}, \overline{y})) \cdot (\omega_2'', \omega_2') = 0. \end{cases}$$

This means that the vector $(I_1(\overline{x}, \overline{y}), -I_2(\overline{x}, \overline{y}))$ is orthogonal to (ω_1'', ω_1') and to (ω_2'', ω_2'). We can consider two cases:

1. The vectors (ω_1'', ω_1') and (ω_2'', ω_2') are orthogonal and coincident (that is, $(\omega_1'', \omega_1') \equiv (\omega_2'', \omega_2')$); see Figure 3.
2. The two vectors (ω_1'', ω_1') and (ω_2'', ω_2') are orthogonal and placed in the opposite direction (that is, $\omega_1'' = -\omega_2''$ and $\omega_1' = -\omega_2'$); see Figure 4.

For both cases we can consider, instead of the two null components of the vector b in (5.2), only one equation (because it is easy to see that in these two cases they are the same). Let us take, for example, the first. That is,

$$I_2(\overline{x}, \overline{y})\omega_1' - I_1(\overline{x}, \overline{y})\omega_1'' = 0. \tag{5.3}$$

Now, to complete the proof, let us consider the definitions of images I_1 and I_2 as in the

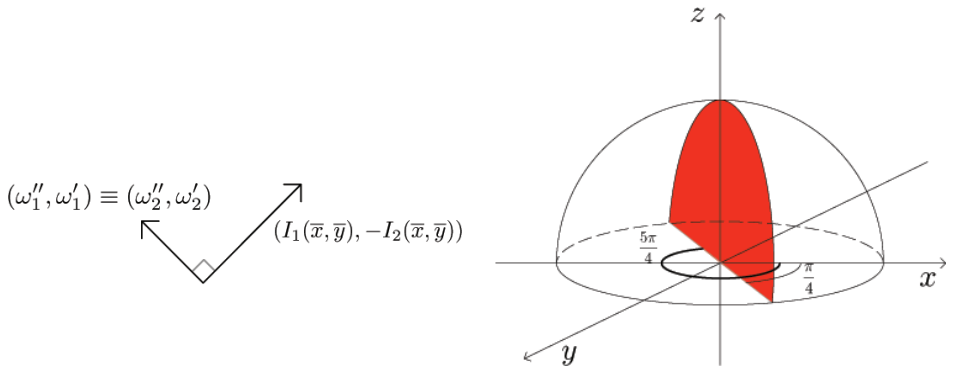

Figure 3. *On the left the position of the orthogonal vector corresponding to the first case. On the right, in red, the set of all the possible light sources corresponding to this situation.*

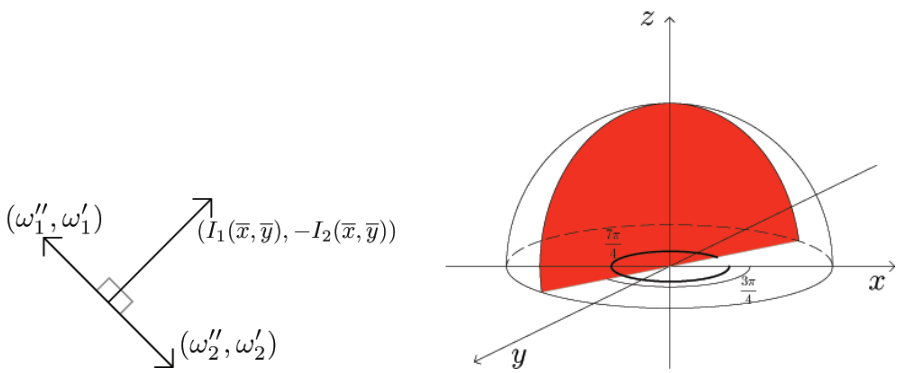

Figure 4. *On the left, the position of the vectors corresponding to the second case. On the right, the set of all the possible light sources in the unitary sphere.*

physical case. By replacing their definitions we have

$$\frac{-\nabla u(\overline{x},\overline{y})\cdot\widetilde{\omega}''+\omega_3''}{\sqrt{1+|\nabla u(\overline{x},\overline{y})|^2}}\omega_1'-\frac{-\nabla u(\overline{x},\overline{y})\cdot\widetilde{\omega}'+\omega_3'}{\sqrt{1+|\nabla u(\overline{x},\overline{y})|^2}}\omega_1''=0,$$

$$\frac{-\nabla u(\overline{x},\overline{y})\cdot(\omega_1'',\omega_2'')+\omega_3''}{\sqrt{1+|\nabla u(\overline{x},\overline{y})|^2}}\omega_1'-\frac{-\nabla u(\overline{x},\overline{y})\cdot(\omega_1',\omega_2')+\omega_3'}{\sqrt{1+|\nabla u(\overline{x},\overline{y})|^2}}\omega_1''=0,$$

$$-\frac{\partial u}{\partial x}(\overline{x},\overline{y})\omega_1''\omega_1'-\frac{\partial u}{\partial y}(\overline{x},\overline{y})\omega_2''\omega_1'+\omega_3''\omega_1'+\frac{\partial u}{\partial x}(\overline{x},\overline{y})\omega_1'\omega_1''+\frac{\partial u}{\partial y}(\overline{x},\overline{y})\omega_2'\omega_1''-\omega_3'\omega_1''=0,$$

$$-\frac{\partial u}{\partial x}(\overline{x},\overline{y})\omega_1''\omega_1'-\frac{\partial u}{\partial y}(\overline{x},\overline{y})\omega_1''\omega_1'+\omega_3''\omega_1'+\frac{\partial u}{\partial x}(\overline{x},\overline{y})\omega_1'\omega_1''+\frac{\partial u}{\partial y}(\overline{x},\overline{y})\omega_1'\omega_1''-\omega_3'\omega_1''=0,$$

which implies

$$\frac{\omega_3''}{\omega_3'}=\frac{\omega_1''}{\omega_1'}=\frac{\omega_2''}{\omega_2'}.$$

Then, using the spherical coordinates for the light source vectors, we get

$$\frac{\cos\varphi_2}{\cos\varphi_1}=\frac{\sin\varphi_2\cos\theta_2}{\sin\varphi_1\cos\theta_1}=\frac{\sin\varphi_2\sin\theta_2}{\sin\varphi_1\sin\theta_1}. \tag{5.4}$$

In the first case we have that $\theta_1, \theta_2 \in \{\frac{\pi}{4}, \frac{5\pi}{4}\}$, whereas in the second case $\theta_1, \theta_2 \in \{\frac{3\pi}{4}, \frac{7\pi}{4}\}$. Our goal is to prove that $\theta_1 = \theta_2$ in order to obtain the contradiction because in this case we have that $\widetilde{\omega}' = \widetilde{\omega}''$ (i.e., $\omega' = \omega''$) and this it is not the case for the photometric stereo technique.

It is clear that, for both cases, if $\frac{\cos\theta_2}{\cos\theta_1} = +1$, then $\theta_1 = \theta_2$, while $\frac{\cos\theta_2}{\cos\theta_1} = -1$ means $\theta_1 \neq \theta_2$.

Let us suppose, by contradiction again, that $\theta_1 \neq \theta_2$. Then, from (5.4) we have

$$\frac{\cos\varphi_2}{\cos\varphi_1} = -\frac{\sin\varphi_2}{\sin\varphi_1} \Rightarrow \tan\varphi_1 = -\tan\varphi_2,$$

which is not possible because $\varphi_1, \varphi_2 \in [0, \frac{\pi}{2}]$. ■

We will see that this lemma will be useful in two important points: in section 5, for the proof of the uniqueness of solution of the problem, and in section 6, for an important remark about the semi-Lagrangian numerical scheme.

It is clear that the structure of the vector field $b(x, y)$ near the point of discontinuity is very important. In fact, the characteristic curves do not have to find obstacles for the propagation of the information across the domain. In Figure 5 we sketched all the possibles cases of behavior of $b(x, y)$ around a point $(\overline{x}, \overline{y})$ belonging to a fixed discontinuity curve $\gamma(t)$. In Figures 5(a) and 5(b) we consider the vector field well structured for the information flow. In the other two cases of Figures 5(c) and 5(d) we are not able to obtain a unique continuous solution without knowing more about the height of the surface on the curve $\gamma(t)$.

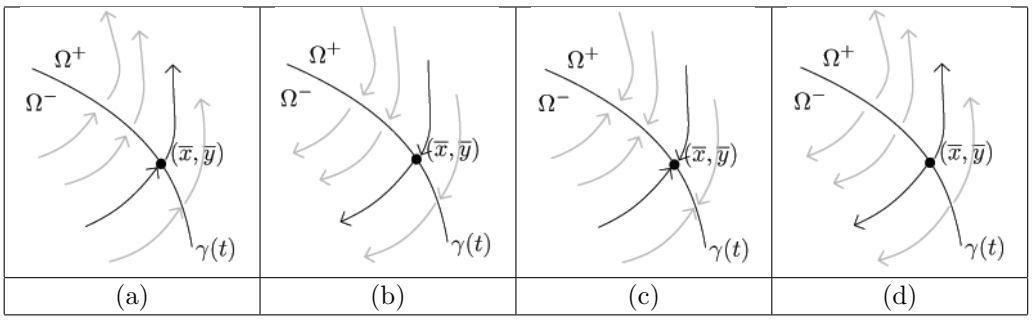

Figure 5. *The vector field with respect to the discontinuity curve $\gamma(t)$.*

Let us start by proving a result describing the global structure of $b(x, y)$. We will emphasize later the importance of this result with respect to the curves of its discontinuity. In fact, it is possible to prove that the characteristic field has the features described in Figure 5(a) or Figure 5(b).

Theorem 5.2. *Let us assume to be in the physical case* (C2)*, and let $\gamma(t)$ be a regular curve of discontinuity for the function $b(x, y)$ (and $f(x, y)$). Let $(\overline{x}, \overline{y}) \in \gamma(t)$, and let $n(\overline{x}, \overline{y})$ be the outgoing normal with respect to the set Ω^+ (located on the right of $\gamma(t)$); then we have*

$$\left[\lim_{\substack{(x,y)\to(\overline{x},\overline{y})\\(x,y)\in\Omega^+}} b(x, y) \cdot n(\overline{x}, \overline{y})\right]\left[\lim_{\substack{(x,y)\to(\overline{x},\overline{y})\\(x,y)\in\Omega^-}} b(x, y) \cdot n(\overline{x}, \overline{y})\right] \geq 0. \tag{5.5}$$

Proof. Let us define the quantities

$$I_1^+ := \lim_{\substack{(x,y)\to(\overline{x},\overline{y})\\(x,y)\in\Omega^+}} I_1(x,y), \qquad I_1^- := \lim_{\substack{(x,y)\to(\overline{x},\overline{y})\\(x,y)\in\Omega^-}} I_1(x,y),$$
$$I_2^+ := \lim_{\substack{(x,y)\to(\overline{x},\overline{y})\\(x,y)\in\Omega^+}} I_2(x,y), \qquad I_2^- := \lim_{\substack{(x,y)\to(\overline{x},\overline{y})\\(x,y)\in\Omega^-}} I_2(x,y).$$

In order to work with the vector field $b(x,y)$ in the neighborhood of $(\overline{x},\overline{y})$, we consider the relations

$$\begin{aligned}\lim_{\substack{(x,y)\to(\overline{x},\overline{y})\\(x,y)\in\Omega^+}} b(x,y) &= (b_1^+, b_2^+) = (I_2^+\omega_1' - I_1^+\omega_1'', I_2^+\omega_2' - I_1^+\omega_2''),\\ \lim_{\substack{(x,y)\to(\overline{x},\overline{y})\\(x,y)\in\Omega^-}} b(x,y) &= (b_1^-, b_2^-) = (I_2^-\omega_1' - I_1^-\omega_1'', I_2^-\omega_2' - I_1^-\omega_2'').\end{aligned} \tag{5.6}$$

Denoting as $(n_1,n_2) = (n_1(\overline{x},\overline{y}), n_2(\overline{x},\overline{y}))$ the two coordinates of $n(\overline{x},\overline{y})$ and replacing (5.6) in the inequality (5.5), we obtain

$$b_1^+b_1^-n_1^2 + b_2^+b_2^-n_2^2 + n_1n_2(b_1^+b_2^- + b_2^+b_1^-) \geq 0,$$

which gives, in explicit terms,

$$\begin{aligned}&(I_2^+\omega_1' - I_1^+\omega_1'')(I_2^-\omega_1' - I_1^-\omega_1'')n_1^2 + (I_2^+\omega_2' - I_1^+\omega_2'')(I_2^-\omega_2' - I_1^-\omega_2'')n_2^2\\ &\quad + \Big[(I_2^+\omega_1' - I_1^+\omega_1'')(I_2^-\omega_2' - I_1^-\omega_2'') + (I_2^-\omega_1' - I_1^-\omega_1'')(I_2^+\omega_2' - I_1^+\omega_2'')\Big]n_1n_2 \geq 0.\end{aligned} \tag{5.7}$$

Let us separate the coefficients that multiply n_1^2 in (5.8), n_2^2 in (5.9), and n_1n_2 in (5.10). We can write them, respectively, as

$$\begin{aligned}&I_2^+I_2^-(\omega_1')^2 - I_2 + I_1^-\omega_1'\omega_1'' - I_1^+I_2^-\omega_1'\omega_1'' + I_1^+I_1^-(\omega_1'')^2\\ &\qquad = I_2^+I_2^-(\omega_1')^2 - (I_2^+I_1^- + I_1^+I_2^-)\omega_1'\omega_1'' + I_1^+I_1^-(\omega_1'')^2,\end{aligned} \tag{5.8}$$

$$\begin{aligned}&I_2^+I_2^-(\omega_2')^2 - I_2^+I_1^-\omega_2'\omega_2'' - I_1^+I_2^-\omega_2'\omega_2'' + I_1^+I_1^-(\omega_2'')^2\\ &\qquad = I_2^+I_2^-(\omega_2')^2 - \omega_2'\omega_2''(I_1^+I_2^- + I_2^+I_1^-) + I_1^+I_1^-(\omega_2'')^2,\end{aligned} \tag{5.9}$$

$$\begin{aligned}&I_2^+I_2^-\omega_1'\omega_2' - I_1^-I_2^+\omega_1'\omega_2'' - I_1^+I_2^-\omega_1''\omega_2' + I_1^+I_1^-\omega_1''\omega_2''\\ &+ I_2^+I_2^-\omega_2'\omega_1' - I_2^+I_1^-\omega_2'\omega_1'' - I_1^+I_2^-\omega_2''\omega_1' + I_1^+I_1^-\omega_1''\omega_2''\\ &= 2I_2^+I_2^-\omega_1'\omega_2' - \omega_1'\omega_2''(I_1^-I_2^+ + I_1^+I_2^-) - \omega_1''\omega_2'(I_1^-I_2^2 + I_1^+I_2^-) + 2I_1^+I_1^-\omega_1''\omega_2''\\ &= 2I_2^+I_2^-\omega_1'\omega_2' - (\omega_1'\omega_2'' + \omega_1''\omega_2')(I_1^-I_2^+ + I_1^+I_2^-) + 2I_1^+I_1^-\omega_1''\omega_2''.\end{aligned} \tag{5.10}$$

To proceed with the proof in the case (C2), we consider the following equality for the image functions:

$$I_1^+ = \lim_{\substack{(x,y)\to(\overline{x},\overline{y})\\(x,y)\in\Omega^+}} I_1(x,y) = \lim_{\substack{(x,y)\to(\overline{x},\overline{y})\\(x,y)\in\Omega^+}} \frac{-\nabla u(x,y)\cdot\widetilde{\omega}' + \omega_3'}{\sqrt{1+|\nabla u(x,y)|^2}} = \frac{-\nabla u^+\cdot\widetilde{\omega}' + \omega_3'}{\sqrt{1+|\nabla u^+|^2}},$$

$$I_1^- = \lim_{\substack{(x,y)\to(\overline{x},\overline{y})\\(x,y)\in\Omega^-}} I_1(x,y) = \lim_{\substack{(x,y)\to(\overline{x},\overline{y})\\(x,y)\in\Omega^-}} \frac{-\nabla u(x,y)\cdot\widetilde{\omega}' + \omega_3'}{\sqrt{1+|\nabla u(x,y)|^2}} = \frac{-\nabla u^-\cdot\widetilde{\omega}' + \omega_3'}{\sqrt{1+|\nabla u^-|^2}},$$

$$I_2^+ = \lim_{\substack{(x,y)\to(\overline{x},\overline{y})\\(x,y)\in\Omega^+}} I_2(x,y) = \lim_{\substack{(x,y)\to(\overline{x},\overline{y})\\(x,y)\in\Omega^+}} \frac{-\nabla u(x,y)\cdot\widetilde{\omega}'' + \omega_3''}{\sqrt{1+|\nabla u(x,y)|^2}} = \frac{-\nabla u^+\cdot\widetilde{\omega}'' + \omega_3''}{\sqrt{1+|\nabla u^+|^2}},$$

$$I_2^- = \lim_{\substack{(x,y)\to(\overline{x},\overline{y})\\(x,y)\in\Omega^-}} I_2(x,y) = \lim_{\substack{(x,y)\to(\overline{x},\overline{y})\\(x,y)\in\Omega^-}} \frac{-\nabla u(x,y)\cdot\widetilde{\omega}'' + \omega_3''}{\sqrt{1+|\nabla u(x,y)|^2}} = \frac{-\nabla u^-\cdot\widetilde{\omega}'' + \omega_3''}{\sqrt{1+|\nabla u^-|^2}}.$$

Note that in the coefficients (5.8), (5.9), and (5.10) all terms are divided by a common denominator

$$\sqrt{1+|\nabla u^+|^2}\sqrt{1+|\nabla u^-|^2}$$

which can be dropped since it is strictly positive. Consider the following quantities (always positive because of the absence of the black shadows):

$$\begin{aligned} i_1^+ &:= -\nabla u^+\cdot\widetilde{\omega}' + \omega_3', \qquad & i_1^- &:= -\nabla u^-\cdot\widetilde{\omega}' + \omega_3',\\ i_2^+ &:= -\nabla u^+\cdot\widetilde{\omega}'' + \omega_3'', \qquad & i_2^- &:= -\nabla u^-\cdot\widetilde{\omega}'' + \omega_3'', \end{aligned} \tag{5.11}$$

and, considering the same differences (as in Theorem 5.4),

$$\begin{aligned} i_1^+ - i_1^- &= -\nabla u^+\cdot\widetilde{\omega}' + \omega_3' + \nabla u^-\cdot\widetilde{\omega}' - \omega_3',\\ i_2^+ - i_2^- &= -\nabla u^+\cdot\widetilde{\omega}'' + \omega_3'' + \nabla u^-\cdot\widetilde{\omega}'' - \omega_3'', \end{aligned} \tag{5.12}$$

we have

$$\begin{aligned} i_1^+ &= i_1^- + \xi\cdot\widetilde{\omega}',\\ i_2^+ &= i_2^- + \xi\cdot\widetilde{\omega}'', \end{aligned} \tag{5.13}$$

where

$$\xi = \nabla u^- - \nabla u^+ = (\xi_1,\xi_2) = \left(\frac{\partial u^-}{\partial x} - \frac{\partial u^+}{\partial x}, \frac{\partial u^-}{\partial y} - \frac{\partial u^+}{\partial y}\right). \tag{5.14}$$

Now, substituting (5.13) into (5.8), (5.9), and (5.10), we obtain, respectively,

$$\begin{aligned} &(i_2^-)^2(\omega_1')^2 + i_2^-(\omega_1')^2\xi\widetilde{\omega}'' + (i_1^-)^2(\omega_1'')^2 + i_1^-(\omega_1'')^2\xi\widetilde{\omega}' - \Big[i_2^-i_1^- + i_1^-\xi\widetilde{\omega}'' + i_1^-i_2^- + i_2^-\xi\widetilde{\omega}'\Big]\omega_1'\omega_1''\\ &= (i_1^-\omega_1'' - i_2^-\omega_1')^2 + \xi\Big[i_2^-(\omega_1')^2\widetilde{\omega}'' + i_1^-(\omega_1'')^2\widetilde{\omega}' - \omega_1'\omega_1''(i_1^-\widetilde{\omega}'' + i_2^-\widetilde{\omega}')\Big]\\ &= (i_2^-\omega_2' - i_1^-\omega_2'')^2 + \xi\Big[(i_1^-\omega_1'' - i_2^-\omega_1')(\widetilde{\omega}'\omega_1'' - \widetilde{\omega}''\omega_1')\Big], \end{aligned}$$

$$
\begin{aligned}
&(i_2^-)^2(\omega_2')^2 + i_2^-(\omega_2')^2\xi\widetilde{\omega}'' + (i_1^-)^2(\omega_2'')^2 + i_1^-(\omega_2'')^2\xi\widetilde{\omega}' - \Big[i_1^-i_2^- + i_2^-\xi\widetilde{\omega}' + i_2^-i_1^- + i_1^-\xi\widetilde{\omega}''\Big]\omega_2'\omega_2'' \\
&= (i_2^-\omega_2' - i_1^-\omega_2'')^2 + \xi\Big[i_2^-(\omega_2')^2\widetilde{\omega}'' - i_1^-(\omega_2'')^2\widetilde{\omega}' - \omega_2'\omega_2''(i_1^-\widetilde{\omega}'' + i_2^-\widetilde{\omega}')\Big] \\
&= (i_2^-\omega_2' - i_1^-\omega_2'')^2 + \xi\Big[(i_1^-\omega_2'' - i_2^-\omega_2')(\widetilde{\omega}'\omega_2'' - \widetilde{\omega}''\omega_2')\Big],
\end{aligned}
$$

$$
\begin{aligned}
&2(i_2^-)^2\omega_1'\omega_2' + 2i_2^-\omega_1'\omega_2'\xi\widetilde{\omega}'' + 2(i_1^-)^2\omega_1''\omega_2'' + 2i_1^-\omega_1''\omega_2''\xi\widetilde{\omega}' \\
&- (\omega_1'\omega_2'' + \omega_1''\omega_2')\Big[i_1^-i_2^- + i_1^-\xi\widetilde{\omega}'' + i_1^-i_2^- + i_2^-\xi\widetilde{\omega}'\Big] \\
&= 2(i_1^-)^2\omega_1''\omega_2'' + 2(i_2^-)^2\omega_1'\omega_2' - 2i_1^-i_2^-(\omega_1'\omega_2'' + \omega_1''\omega_2') \\
&+ \xi\Big[2i_2^-\omega_1'\omega_2'\widetilde{\omega}'' + 2i_1^-\omega_1''\omega_2''\widetilde{\omega}' - (\omega_1'\omega_2'' + \omega_1''\omega_2')(i_1^-\widetilde{\omega}'' + i_2^-\widetilde{\omega}')\Big] \\
&= -2i_1^-i_2^-\omega_1''\omega_2' + 2(i_1^-)^2\omega_1''\omega_2'' + 2(i_2^-)^2\omega_1'\omega_2' - 2i_1^-i_2^-\omega_1'\omega_2'' \\
&+ \xi\Big[2i_2^-\omega_1'\omega_2'\widetilde{\omega}'' + 2i_1^-\omega_1''\omega_2''\widetilde{\omega}' - (\omega_1'\omega_2'' + \omega_1''\omega_2')(i_1^-\widetilde{\omega}'' + i_2^-\widetilde{\omega}')\Big] \\
&= -2(i_1^-\omega_1'' - i_2\omega_1')(i_2^-\omega_2' - i_1^-\omega_2'') \\
&+ \xi\Big[2i_2^-\omega_1'\omega_2'\widetilde{\omega}'' + 2i_1^-\omega_1''\omega_2''\widetilde{\omega}' - (\omega_1'\omega_2'' + \omega_1''\omega_2')(i_1^-\widetilde{\omega}'' + i_2^-\widetilde{\omega}')\Big].
\end{aligned}
$$

Substituting them into (5.7), we have

$$
\begin{aligned}
&\Big[(i_1^-\omega_1'' - i_2^-\omega_1')n_1 - (i_2^-\omega_2' - i_1^-\omega_2'')n_2\Big]^2 \\
&+ \xi\Big[(i_1^-\omega_1'' - i_2^-\omega_1')(\widetilde{\omega}'\omega_1'' - \widetilde{\omega}''\omega_1')n_1^2 + (i_1^-\omega_2'' - i_2^-\omega_2')(\widetilde{\omega}'\omega_2'' - \widetilde{\omega}''\omega_2')n_2^2 \\
&+ \big(2i_2^-\omega_1'\omega_2'\widetilde{\omega}'' + 2i_1^-\omega_1''\omega_2''\widetilde{\omega}' - (\omega_1'\omega_2'' + \omega_1''\omega_2')(i_1^-\widetilde{\omega}'' + i_2^-\widetilde{\omega}')\big)n_1n_2\Big] \geq 0.
\end{aligned}
$$

In order to verify the previous inequality we continue to manipulate the left side, obtaining after some algebra

$$
\begin{aligned}
&[i_2^-(n_1\omega_1' + n_2\omega_2') - i_1^-(n_1\omega_1'' + n_2\omega_2'')] \\
&\qquad [i_2^-(n_1\omega_1' + n_2\omega_2') - i_1^-(n_1\omega_1'' + n_2\omega_2'') - (n_1\xi_2 - n_2\xi_1)(\omega_1''\omega_2' - \omega_1'\omega_2'')] \geq 0.
\end{aligned} \tag{5.15}
$$

In order to conclude the proof, let us emphasize that

$$
(n_1\xi_2 - n_2\xi_1) \equiv 0. \tag{5.16}
$$

Using (5.14) we can write the previous equivalence as follows:

$$
\begin{aligned}
n_1\xi_2 - n_2\xi_1 &= n_1\left(\frac{\partial u^-}{\partial y} - \frac{\partial u^+}{\partial y}\right) - n_2\left(\frac{\partial u^-}{\partial x} - \frac{\partial u^+}{\partial x}\right) = -\frac{\partial u^-}{\partial x}n_2 + \frac{\partial u^-}{\partial y}n_1 - \left(-\frac{\partial u^+}{\partial x}n_2 + \frac{\partial u^+}{\partial y}n_1\right) \\
&= \lim_{\substack{(x,y)\to(\overline{x},\overline{y}) \\ (x,y)\in\Omega^-}} \nabla_{(-n_2,n_1)}u(x,y) - \lim_{\substack{(x,y)\to(\overline{x},\overline{y}) \\ (x,y)\in\Omega^+}} \nabla_{(-n_2,n_1)}u(x,y) = \frac{\partial u^-}{\partial t}(\overline{x},\overline{y}) - \frac{\partial u^+}{\partial t}(\overline{x},\overline{y}) = 0,
\end{aligned} \tag{5.17}
$$

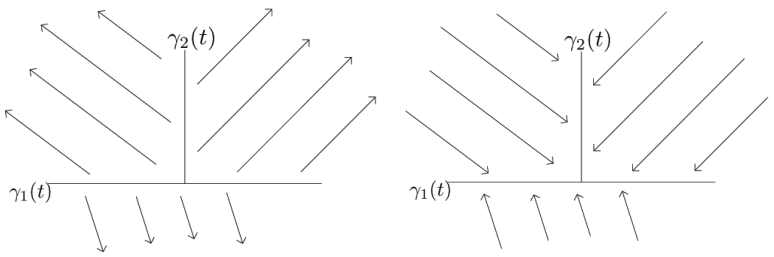

Figure 6. *Two examples of impossible structures for the vector field $b(x, y)$.*

where in the last passage we use the orthogonality of $(-n_2, n_1)$ with respect to the normal vector (n_1, n_2) of the discontinuity curve $\gamma(t)$. This means that we have to consider the gradient in the tangential direction with respect to $\gamma(t)$ for both sides Ω^+ and Ω^-, that is, $\frac{\partial u^+}{\partial t}$ and $\frac{\partial u^-}{\partial t}$. Now, since we are assuming the continuity for the surface u, we have that these two derivatives are equal for all the points $(\overline{x}, \overline{y})$.

Finally, from (5.15) we arrive at

$$[i_2^-(n_1\omega_1' + n_2\omega_2') - i_1^-(n_1\omega_1'' + n_2\omega_2'')]^2 \geq 0,$$

which ends the proof. ■

The conclusion of the previous theorem is related to the structure of the vector field $b(x, y)$. In fact, near the points of discontinuity, the condition (5.21) allows us to respect the structure represented in Figures 5(a) and 5(b). If we consider intersection of discontinuity curves, it is clear that some behaviors (as in Figure 6) for $b(x, y)$ cannot appear. However, this condition on the vector field b is necessary for the construction of a unique Lipschitz solution shown in the following theorem.

Theorem 5.3. *Let us assume to be in the physical case* (C2)*. Consider the problem*

$$\begin{cases} b(x,y)\cdot\nabla u(x,y) = f(x,y) & a.e.\ (x,y)\in\Omega, \\ u(x,y) = g(x,y) & \forall (x,y)\in\partial\Omega. \end{cases} \tag{5.18}$$

Let us suppose that $(\gamma_1(t), \ldots, \gamma_k(t))$, the family of regular discontinuous curves for $b(x, y)$ and $f(x, y)$, are not characteristic curves (with respect to the previous problem). Then, there exists a unique Lipschitz solution of (5.18)*.*

Proof. As said before, in order to prove the uniqueness of a Lipschitz solution, we consider the characteristic method. For problem (5.18) the characteristics are given by

$$\begin{cases} \text{(a)} & \dot{x}_c(s) = b_1(x_c(s), y_c(s)), \\ \text{(b)} & \dot{y}_c(s) = b_2(x_c(s), y_c(s)), \\ \text{(c)} & \dot{z}(s) = f(x_c(s), y_c(s)), \end{cases} \tag{5.19}$$

where s is the variable of the parameterization and $z(s)$ is the value of u on the projected characteristic (that is, $z(s) = u(x_c(s), y_c(s))$).

The initial condition for integrating this system of ordinary differential equations is taken from the values of the function u known on the boundary $\Gamma_{in} := \{x \in \Gamma = \partial\Omega : b \cdot n \leq 0\}$.

Then

$$\begin{cases} (\mathrm{a}_0) & x_c(0) = x_0, \\ (\mathrm{b}_0) & y_c(0) = y_0, \\ (\mathrm{c}_0) & u(x_c(0), y_c(0)) = g(x_0, y_0) \end{cases}$$

with $(x_0, y_0) \in \partial\Omega$. It is possible now to use the result (5.1), given that there is no possibility of having pits or source points in the domain Ω since the vector field $b(x, y)$ is always different from the null vector inside this domain.

Starting from the boundary, it is possible to integrate until the first point of intersection between the projection of the characteristic and the first jump discontinuity curve using the standard method [13]. Let us consider the point $(x_1, y_1) \in \gamma_j$ to also be a point of the characteristic passing through (x_0, y_0); that is, there exist $\bar{s}$ and $\bar{t}_j$ such that $(x_1, y_1) = (x_c(\bar{s}), y_c(\bar{s})) = \gamma_j(\bar{t}_j)$ (see Figure 7).

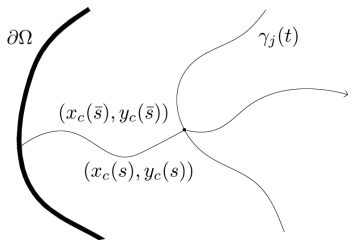

Figure 7. *A schematic representation of a first intersection point $(x_c(\bar{s}), y_c(\bar{s}))$ between the projected characteristic and the curve of discontinuity $\gamma(t)$.*

Now we can begin to solve another Dirichlet problem on the characteristic, very similar to the starting one:

$$\begin{cases} b(x, y) \cdot \nabla u(x, y) = f(x, y) & \forall (x, y) \in (x_c(s), y_c(s)) \text{ with } s > \bar{s}, \\ u(x_c(\bar{s}), y_c(\bar{s})) = \lim_{s \to \bar{s}} u(x_c(s), y_c(s)). \end{cases} \tag{5.20}$$

The well-posedness of (5.20) is guaranteed from the type of discontinuity of the functions $b(x, y)$ and $f(x, y)$. In fact, the jump discontinuity allows us to work with prolongation by the limit. We are considering the problem only on a specific characteristic taking as initial starting value the limit of $z(s)_{s \to \bar{s}}$ for the system of ordinary differential equation (5.19). Using Theorem 5.2, it is possible to understand that we do not need additional information about the solution u inside the domain. In fact, the only information we need to reconstruct the surface over all the domain Ω is the Dirichlet boundary condition.

The argument can be extended to all discontinuity points, that is, for all the points of $(\gamma_1(t), \dots \gamma_k(t))$. This means that the integration along the characteristic $s > \bar{s}$ is intended until a new point of discontinuity of the functions $b(x, y)$ and $f(x, y)$, that is, until a new intersection point between the characteristic and one of the γ_i curves. ■

Theorem 5.4. *Let us assume to be in the physical case* (C2)*, and let $(\gamma_1(t), \dots, \gamma_k(t))$ be the family of jump discontinuity curves for b (i.e., for I_1 and I_2). Then for every two distinct points $(\widehat{x}, \widehat{y})$, $(\bar{x}, \bar{y}) \in \Omega \backslash (\gamma_1(t), \dots, \gamma_k(t))$ we have*

$$b(\widehat{x}, \widehat{y}) \cdot b(\bar{x}, \bar{y}) \geq 0. \tag{5.21}$$

Proof. We define the quantities

$$\widehat{I}_1 := I_1(\widehat{x},\widehat{y}), \quad \bar{I}_1 := I_1(\bar{x},\bar{y}),$$
$$\widehat{I}_2 := I_2(\widehat{x},\widehat{y}), \quad \bar{I}_2 := I_2(\bar{x},\bar{y}),$$

we replace them in the analytical form of $b(x,y)$ (4.9) as

$$\widehat{b} := (b_1(\widehat{x},\widehat{y}), b_2(\widehat{x},\widehat{y})) = (\widehat{I}_2\omega_1' - \widehat{I}_1\omega_1'', \widehat{I}_2\omega_2' - \widehat{I}_1\omega_2''),$$
$$\bar{b} := (b_1(\bar{x},\bar{y}), b_2(\bar{x},\bar{y})) = (\bar{I}_2\omega_1' - \bar{I}_1\omega_1'', \bar{I}_2\omega_2' - \bar{I}_1\omega_2''),$$

and we write (5.21) in explicit terms as

$$(\widehat{I}_2\omega_1' - \widehat{I}_1\omega_1'', \widehat{I}_2\omega_2' - \widehat{I}_1\omega_2'') \cdot (\bar{I}_2\omega_1' - \bar{I}_1\omega_1'', \bar{I}_2\omega_2' - \bar{I}_1\omega_2'') \geq 0,$$
$$(\widehat{I}_2\omega_1' - \widehat{I}_1\omega_1'')(\bar{I}_2\omega_1' - \bar{I}_1\omega_1'') + (\widehat{I}_2\omega_2' - \widehat{I}_1\omega_2'')(\bar{I}_2\omega_2' - \bar{I}_1\omega_2'') \geq 0.$$

We get

$$\widehat{I}_2\bar{I}_2(\omega_2')^2 - \bar{I}_1\widehat{I}_2\omega_1'\omega_1'' - \widehat{I}_1\bar{I}_2\omega_1'\omega_1'' + \widehat{I}_1\bar{I}_1(\omega_1'')^2 + \widehat{I}_2\bar{I}_2(\omega_2')^2 - \bar{I}_1\widehat{I}_2\omega_2'\omega_2'' - \widehat{I}_1\bar{I}_2\omega_2'\omega_2'' + \widehat{I}_1\bar{I}_1(\omega_2'')^2 \geq 0,$$

and reordering the terms we get

$$\widehat{I}_2\bar{I}_2((\omega_1')^2 + (\omega_2')^2) - \bar{I}_1\widehat{I}_2(\omega_1'\omega_1'' + \omega_2'\omega_2'') - \widehat{I}_1\bar{I}_2(\omega_1'\omega_1'' + \omega_2'\omega_2'') + \widehat{I}_1\bar{I}_1((\omega_1'')^2 + (\omega_2'')^2) \geq 0,$$

which can be written in compact form as

$$\widehat{I}_2\bar{I}_2|\widetilde{\omega}'|^2 + \widehat{I}_1\bar{I}_1|\widetilde{\omega}''|^2 \geq (\widehat{I}_1\bar{I}_2 + \bar{I}_1\widehat{I}_2)\widetilde{\omega}' \cdot \widetilde{\omega}''. \tag{5.22}$$

Now we have to take into account that our images all have bounded values in $(0,1]$. The only way to have the left side of (5.22) equal to zero is to take $\widetilde{\omega}'$ and $\widetilde{\omega}''$ such that $|\widetilde{\omega}'|$ and $|\widetilde{\omega}''|$ are equal to zero at the same time. But this is not permitted by the photometric stereo technique definition used to solve the problem (because the direction of the light sources must be different).

It is clear that if we take the two light directions such that $\widetilde{\omega}' \cdot \widetilde{\omega}'' \leq 0$, condition (5.21) is verified, but now we want to prove it (through the (5.22) formulation) in a more general case.

Let us define the following quantities:

$$\widehat{I}_1 = \frac{-\nabla u(\widehat{x},\widehat{y}) \cdot \widetilde{\omega}' + \omega_3'}{\sqrt{1 + |\nabla u(\widehat{x},\widehat{y})|^2}}, \qquad \bar{I}_1 = \frac{-\nabla u(\bar{x},\bar{y}) \cdot \widetilde{\omega}' + \omega_3'}{\sqrt{1 + |\nabla u(\bar{x},\bar{y})|^2}},$$
$$\widehat{I}_2 = \frac{-\nabla u(\widehat{x},\widehat{y}) \cdot \widetilde{\omega}'' + \omega_3''}{\sqrt{1 + |\nabla u(\widehat{x},\widehat{y})|^2}}, \qquad \bar{I}_2 = \frac{-\nabla u(\bar{x},\bar{y}) \cdot \widetilde{\omega}'' + \omega_3''}{\sqrt{1 + |\nabla u(\bar{x},\bar{y})|^2}}.$$

Substituting them into (5.22), we observe that the denominator of all the terms on both sides is the same, that is,

$$\sqrt{1 + |\nabla u(\bar{x},\bar{y})|^2}\sqrt{1 + |\nabla u(\widehat{x},\widehat{y})|^2},$$

and we can study the inequality without it because it is always positive. The quantities

$$\begin{aligned} \widehat{i}_1 &= -\nabla u(\widehat{x},\widehat{y})\cdot\widetilde{\omega}' + \omega_3', \qquad \bar{i}_1 = -\nabla u(\bar{x},\bar{y})\cdot\widetilde{\omega}' + \omega_3', \\ \widehat{i}_2 &= -\nabla u(\widehat{x},\widehat{y})\cdot\widetilde{\omega}'' + \omega_3'', \qquad \bar{i}_2 = -\nabla u(\bar{x},\bar{y})\cdot\widetilde{\omega}'' + \omega_3'' \end{aligned} \tag{5.23}$$

are positive by definition, and it is possible to calculate the differences as

$$\begin{aligned} \widehat{i}_1 - \bar{i}_1 &= -\nabla u(\widehat{x},\widehat{y})\cdot\widetilde{\omega}' + \omega_3' + \nabla u(\bar{x},\bar{y})\cdot\widetilde{\omega}' - \omega_3', \\ \widehat{i}_2 - \bar{i}_2 &= -\nabla u(\widehat{x},\widehat{y})\cdot\widetilde{\omega}'' + \omega_3'' + \nabla u(\bar{x},\bar{y})\cdot\widetilde{\omega}'' - \omega_3''. \end{aligned} \tag{5.24}$$

Defining $\xi := \nabla u(\bar{x},\bar{y}) - \nabla u(\widehat{x},\widehat{y})$, we have

$$\begin{aligned} \widehat{i}_1 &= \bar{i}_1 + \xi\cdot\widetilde{\omega}', \\ \widehat{i}_2 &= \bar{i}_2 + \xi\cdot\widetilde{\omega}''. \end{aligned} \tag{5.25}$$

Substituting the previous equalities for $\widehat{i}_1$ and $\widehat{i}_2$ into (5.22),

$$\begin{gathered} (\bar{i}_2+\xi\widetilde{\omega}'')\bar{i}_2|\widetilde{\omega}'|^2 + (\bar{i}_1+\xi\widetilde{\omega}')\bar{i}_1|\widetilde{\omega}''|^2 - \Big[(\bar{i}_1+\xi\widetilde{\omega}')\bar{i}_2 + (\bar{i}_2+\xi\widetilde{\omega}'')\bar{i}_1\Big]\widetilde{\omega}'\cdot\widetilde{\omega}'' \geq 0, \\ (\bar{i}_2)^2|\widetilde{\omega}'|^2 + \bar{i}_2|\widetilde{\omega}'|^2\xi\widetilde{\omega}'' + (\bar{i}_1)^2|\widetilde{\omega}''|^2 + \bar{i}_1|\widetilde{\omega}''|^2\xi\widetilde{\omega}' - \Big[\bar{i}_1\bar{i}_2 + \bar{i}_2\xi\widetilde{\omega}' + \bar{i}_1\bar{i}_2 + \bar{i}_1\xi\widetilde{\omega}''\Big]\widetilde{\omega}'\cdot\widetilde{\omega}'' \geq 0, \\ (\bar{i}_2\widetilde{\omega}' - \bar{i}_1\widetilde{\omega}'')^2 + \xi\Big[\bar{i}_2|\widetilde{\omega}'|^2\widetilde{\omega}'' + \bar{i}_1|\widetilde{\omega}''|^2\widetilde{\omega}' - (\bar{i}_2\widetilde{\omega}' + \bar{i}_1\widetilde{\omega}'')\widetilde{\omega}'\cdot\widetilde{\omega}''\Big] \geq 0, \\ (\bar{i}_2\widetilde{\omega}' - \bar{i}_1\widetilde{\omega}'')^2 + \xi\Big[\bar{i}_2|\widetilde{\omega}'|^2\widetilde{\omega}'' + \bar{i}_1|\widetilde{\omega}''|^2\widetilde{\omega}' - \bar{i}_2|\widetilde{\omega}'|^2\widetilde{\omega}'' - \bar{i}_1|\widetilde{\omega}''|^2\widetilde{\omega}''\Big] \geq 0, \\ (\bar{i}_2\widetilde{\omega}' - \bar{i}_1\widetilde{\omega}'')^2 \geq 0, \end{gathered}$$

which is obviously always verified. ■

The previous result is very important in terms of the propagation of information since it says that the vector field b does not have strong changes of direction in the image domain. Especially for the numerical schemes, this result will permit us to obtain good results of approximation even if the interpolation formula will be stopped at order one.

Now we explain why Lipschitz continuous solutions have the minimum regularity required for this type of SfS model. Let us consider the problem in the physical case, where it is easier to understand why a discontinuous function cannot be a solution of problem (5.18). Let us consider the 1D problem, taking, for example, the two functions

$$u_1(x) = \begin{cases} x+1 & \text{if } x \leq 1, \\ -x+3 & \text{if } x > 1, \end{cases} \qquad u_2(x) = \begin{cases} x+1 & \text{if } x \leq 1, \\ -x+2 & \text{if } x > 1. \end{cases}$$

If we choose a light source directions ω such that there are no shadows for both surfaces, then it is possible to write the corresponding relations

$$I(u_1(x)) = \frac{(-u_1'(x),1)}{\sqrt{1+(u_1'(x)^2)}}\cdot(\omega_1,\omega_2) = \frac{(-u_2'(x),1)}{\sqrt{1+(u_2'(x)^2)}}\cdot(\omega_1,\omega_2) = I(u_2(x)).$$

This is because the derivative of $u_1(x)$ and $u_2(x)$ (where they are regular) coincide.

It is clear that these two functions, when we fix the Ω domain, are different on the boundary $\partial\Omega$. However, we will see in the next section that not all the values at the boundary are necessary to identify the solution. Following the previous constructive proof to obtain a weak solution, we need to know the values at the jump of u at every point of discontinuity to identify the solution. This strong limitation implies that this kind of SfS model will not be able to handle discontinuous solutions since, using a light source at infinity, it is impossible to distinguish different discontinuous surfaces which have the same derivative.

5.1. Boundary conditions for the SfS-PS model. In this section we want to introduce the concept of consistent boundary conditions and show how this notion can be useful for the solution of our differential problem. Let us start by showing the role of boundary conditions in our model.

5.1.1. The role of boundary conditions. Let us now focus our attention on the importance of the boundary conditions. It is well known that from the orthographic point of view of the SfS problem, if no boundary conditions are considered, there is a nonuniqueness due to the fact that if $u(x,y)$ is a solution, then $u(x,y)+c$ ($c\in\mathbb{R}$) are also solutions of the same problem. For the SfS-PS problem, we have another kind of inconvenience which gives rise to an ill-posed problem.

A simple example. We consider a first example proposed in [31], where we have two surfaces $u^0_+(x,y)$ and $u^0_-(x,y)$ defined as

$$\begin{cases} u^0_+(x,y) = s(x) + r(y), \\ u^0_-(x,y) = -s(x) + r(y), \end{cases} \tag{5.26}$$

where $s(x), r(y) \in \mathrm{Lip}(\Omega)$. The unit normals to these surfaces, defined a.e., are

$$\begin{cases} n^0_+(x,y) = \dfrac{1}{\sqrt{s'(x)^2 + r'(y)^2 + 1}}\,(-s'(x), -r'(y), 1), \\ n^0_-(x,y) = \dfrac{1}{\sqrt{s'(x)^2 + r'(y)^2 + 1}}\,(s'(x), -r'(y), 1). \end{cases} \tag{5.27}$$

It is very easy to see that the images of both surfaces coincide for the light directions:

$$\omega^0_\varphi = (0, \sin\varphi, \cos\varphi), \quad \varphi \in \left(-\frac{\pi}{2}, \frac{\pi}{2}\right); \tag{5.28}$$

in fact,

$$\omega^0_\varphi \cdot n^0_+(x,y) = \frac{-r'(y)\sin\varphi + \cos\varphi}{\sqrt{s'(x)^2 + r'(y)^2 + 1}} = \omega^0_\varphi \cdot n^0_-(x,y). \tag{5.29}$$

This means that if we choose two angles φ_1 and φ_2, we have to solve the following nonlinear system:

$$\begin{cases} \dfrac{-r'(y)\sin\varphi_1 + \cos\varphi_1}{\sqrt{s'(x)^2 + r'(y)^2 + 1}} = I_1(x,y) \quad \text{a.e. } (x,y)\in\Omega, \\ \dfrac{-r'(y)\sin\varphi_2 + \cos\varphi_2}{\sqrt{s'(x)^2 + r'(y)^2 + 1}} = I_2(x,y) \quad \text{a.e. } (x,y)\in\Omega, \end{cases} \tag{5.30}$$

where the equations are redundant. In this case the system admits at least two solutions, namely $u^0_+(x,y)$ and $u^0_-(x,y)$, that differ just for the boundary condition.

The same ambiguity appears when taking the surfaces

$$\begin{cases} u^{\frac{\pi}{2}}_+(x,y) = s(x) + r(y), \\ u^{\frac{\pi}{2}}_-(x,y) = s(x) - r(y), \end{cases} \tag{5.31}$$

which have the unit normals

$$\begin{cases} n^{\frac{\pi}{2}}_+(x,y) = \dfrac{1}{\sqrt{s'(x)^2 + r'(y)^2 + 1}}\,(-s'(x), -r'(y), 1), \\ n^{\frac{\pi}{2}}_-(x,y) = \dfrac{1}{\sqrt{s'(x)^2 + r'(y)^2 + 1}}\,(-s'(x), r'(y), 1). \end{cases} \tag{5.32}$$

Given the light sources

$$\omega^{\frac{\pi}{2}}_{\varphi} = (\sin\varphi, 0, \cos\varphi), \quad \varphi \in \left(-\frac{\pi}{2}, \frac{\pi}{2}\right), \tag{5.33}$$

we have the same gray-level images; in fact,

$$\omega^{\frac{\pi}{2}}_{\varphi} \cdot n^{\frac{\pi}{2}}_+(x,y) = \frac{-s'(y)\sin\varphi + \cos\varphi}{\sqrt{s'(x)^2 + r'(y)^2 + 1}} = \omega^{\frac{\pi}{2}}_{\varphi} \cdot n^{\frac{\pi}{2}}_-(x,y). \tag{5.34}$$

A rather general example. Now since in the orthographic model the camera is placed at infinity with respect to the surface, it is clear that the previous two cases can be generalized given a surface rotation of an arbitrary angle (namely θ) with respect to the z axis.

Let us start by defining two parametric surfaces h^θ_+ and h^θ_- as a generic rotation of the functions u^0_+ and u^0_- of an angle θ with respect to the z axis, that is,

$$\begin{aligned} h^\theta_+(x,y) &= \begin{pmatrix} \cos\theta & -\sin\theta & 0 \\ \sin\theta & \cos\theta & 0 \\ 0 & 0 & 1 \end{pmatrix} \begin{pmatrix} x \\ y \\ s(x) + r(y) \end{pmatrix} = \begin{pmatrix} x\cos\theta - y\sin\theta \\ x\sin\theta + y\cos\theta \\ s(x) + r(y) \end{pmatrix}, \\ h^\theta_-(x,y) &= \begin{pmatrix} \cos\theta & -\sin\theta & 0 \\ \sin\theta & \cos\theta & 0 \\ 0 & 0 & 1 \end{pmatrix} \begin{pmatrix} x \\ y \\ -s(x) + r(y) \end{pmatrix} = \begin{pmatrix} x\cos\theta - y\sin\theta \\ x\sin\theta + y\cos\theta \\ -s(x) + r(y) \end{pmatrix}. \end{aligned} \tag{5.35}$$

Consider the change of variables

$$\begin{cases} \xi = x\cos\theta - y\sin\theta, \\ \eta = x\sin\theta + y\cos\theta, \end{cases} \tag{5.36}$$

which corresponds to

$$\begin{cases} x = \eta\sin\theta + \xi\cos\theta, \\ y = \eta\cos\theta - \xi\sin\theta, \end{cases} \tag{5.37}$$

and write h^θ_+ and h^θ_- as follows:

$$\begin{aligned} h^\theta_+(\xi,\eta) &= (\xi,\eta, s(\eta\sin\theta+\xi\cos\theta)+r(\eta\cos\theta-\xi\sin\theta)),\\ h^\theta_-(\xi,\eta) &= (\xi,\eta,-s(\eta\sin\theta+\xi\cos\theta)+r(\eta\cos\theta-\xi\sin\theta)). \end{aligned} \tag{5.38}$$

If we also consider the light source depending on a parameter θ as

$$\omega^\theta_\varphi = \left(\cos\left(\theta+\frac{\pi}{2}\right)\sin\varphi, \sin\left(\theta+\frac{\pi}{2}\right)\sin\varphi, \cos\varphi\right) = (-\sin\theta\sin\varphi, \cos\theta\sin\varphi, \cos\varphi), \tag{5.39}$$

it is easy to see that the previous two cases can be obtained by choosing two specific rotations, that is, $\theta = 0$ and $\theta = \frac{\pi}{2}$.

A generalization of the previous ambiguity can be obtained by just verifying that $n^\theta_+ \cdot \omega^\theta_\varphi = n^\theta_- \cdot \omega^\theta_\varphi$ for all θ. Fixing θ and computing the normal vectors n^θ_+ and n^θ_-, we get

$$\begin{aligned} n^\theta_+ &= \frac{(-s\cos\theta+r\sin\theta, -s\sin\theta-r\cos\theta, 1)}{\sqrt{(-s\cos\theta+r\sin\theta)^2+(-s\sin\theta-r\cos\theta)^2+1}} = \frac{(-s\cos\theta+r\sin\theta, -s\sin\theta-r\cos\theta, 1)}{\sqrt{s^2+r^2+1}},\\ n^\theta_- &= \frac{(s\cos\theta+r\sin\theta, s\sin\theta-r\cos\theta, 1)}{\sqrt{(s\cos\theta+r\sin\theta)^2+(s\sin\theta-r\cos\theta)^2+1}} = \frac{(s\cos\theta+r\sin\theta, s\sin\theta-r\cos\theta, 1)}{\sqrt{s^2+r^2+1}}. \end{aligned} \tag{5.40}$$

To verify that both normal vectors lead to the same image, we consider a generic light direction ω^θ_φ. Subtracting, we get

$$\begin{aligned} &n^\theta_+ \cdot \omega^\theta_\varphi - n^\theta_- \cdot \omega^\theta_\varphi\\ &= \frac{-\sin\theta\sin\varphi(-s\cos\theta+r\sin\theta)+\cos\theta\sin\varphi(-s\sin\theta-r\cos\theta)+\cos\varphi}{\sqrt{s^2+r^2+1}}\\ &-\frac{-\sin\theta\sin\varphi(s\cos\theta+r\sin\theta)+\cos\theta\sin\varphi(s\sin\theta-r\cos\theta)+\cos\varphi}{\sqrt{s^2+r^2+1}} = 0. \end{aligned} \tag{5.41}$$

The above remarks show that the role of the boundary conditions is crucial in characterizing a unique solution even for the SfS-PS problem.

5.1.2. Consistent boundary conditions. In the previous section we presented a way to find the unique solution using the characteristic field across all the domain Ω. This approach can be used in two different ways depending on the direction of the characteristic field that we want take into account.

If we call $\nu(x,y)$ the unit outgoing normal vector to $\partial\Omega$, it is possible to define the following subsets of $\partial\Omega$:

$$\Gamma_{in} = \left\{(\widetilde{x},\widetilde{y}) \in \partial\Omega : \nu(\widetilde{x},\widetilde{y}) \cdot \lim_{\substack{(x,y)\to(\widetilde{x},\widetilde{y})\\(x,y)\in\Omega}} b(x,y) \le 0\right\},$$

$$\Gamma_{out} = \Gamma \setminus \Gamma_{in},$$

which are, respectively, the sets of points where the characteristic field is incoming and outgoing with respect to Ω. Let us recall that, in our hypotheses, the vector field b is not continuous.

This means that in all the discontinuous points of b belonging to $\partial\Omega$ we have to consider the limit vector from the inside of the domain. Let us emphasize once more that Theorem 5.2 clarifies also some ambiguous cases for Γ_{in} and Γ_{out}. In fact, if a curve of discontinuity coincides on a part of the boundary, we have to consider the limit vector of $b(x, y)$.

Then, we can write

$$\partial\Omega = \Gamma_{out} \cup \Gamma_{in}.$$

Let us explain what happens in a simple case going back to a previous example where the light sources are $\omega' = (0, 0, 1)$ and $\omega'' = (\sin(\varphi)\cos(\theta), \sin(\theta)\sin(\varphi), \cos(\varphi))$. Then, the vector field that defines the characteristic field, that is, $b(x, y) = (-I_1(x, y)\omega_1'', -I_1(x, y)\omega_2'') = -I_1(x, y)\widetilde{\omega}''$, can be represented by straight lines all parallel to $\widetilde{\omega}''$ but with the head on the opposite side of it. In this case it is possible to see the two sets Γ_{in} and Γ_{out} of a particular domain Ω (i.e., image domain) as in Figure 8.

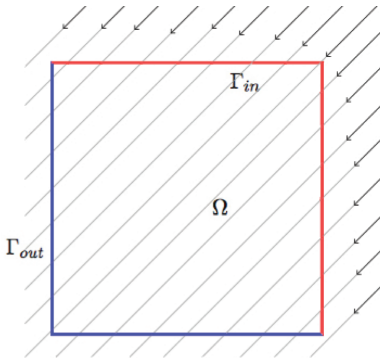

Figure 8. *Domain Ω and the distribution of the Γ_{in} and Γ_{out} sets considering a constant characteristic field (represented by the arrows) as in the previous example.*

As we have seen before, we get to the uniqueness of the weak solution through the characteristic method. In the proof we have not specified the orientation of this vector field, assuming the direction we consider is orientated as the vector field b. In other words, the problem we solved in the proof is the *forward problem*, that is,

$$\begin{cases} b(x, y) \cdot \nabla u(x, y) = f(x, y) & \text{a.e. } (x, y) \in \Omega, \\ u(x, y) = g_{in}(x, y) & \forall (x, y) \in \Gamma_{in}. \end{cases} \tag{5.42}$$

In the same way we can consider the opposite direction and repeat the proof of the uniqueness theorem, obtaining the same result. Let us consider then the following *backward problem*:

$$\begin{cases} -b(x, y) \cdot \nabla u(x, y) = -f(x, y) & \text{a.e. } (x, y) \in \Omega, \\ u(x, y) = g_{out}(x, y) & \forall (x, y) \in \Gamma_{out}. \end{cases} \tag{5.43}$$

It is clear that, when we consider a global boundary condition $g(x, y)$ (as in the general problem (5.18)) defined over all the boundary domain $\partial\Omega$, we need to define the consistency of this function with both of the previous cases. That is, when we start to solve the solution from Γ_{in}, for example, we need to obtain, through the characteristic method, the exact value

of $g(x,y)$ on the "other side" of the boundary, that is, Γ_{out}. With the aim of defining the condition of compatibility of this boundary condition, we will define all the constraints that it has to respect to make the problem well-posed.

Let us emphasize that all the points of Ω which are not points of discontinuity for b can be reached by a characteristic curve; that is, for all these points the solution can be determined in a unique way. We start by considering (5.42). We denote by $\beta(t;x_0,y_0)$ the characteristic curve passing through $(x_0,y_0) \in \Gamma_{in}$ and $(x_1,y_1) \in \Gamma_{out} \cap \beta(t;x_0,y_0)$. Now, following the characteristic method, we determine the value of u_{in} at point (x_1,y_1). Fixing $g_{in}(x_1,y_1) = u_{in}(x_1,y_1)$, we obtain the boundary condition $g_{in}(x,y)$ defined in $\Gamma_{in} \cup \Gamma_{out}$. Let us call it $\overline{g}_{in}(x,y)$. We can repeat this argument to build $\overline{g}_{out}(x,y)$ defined in $\Gamma_{in} \cup \Gamma_{out}$.

Definition 5.5. *A function $g(x,y) \in C(\Gamma_{in}) \cap C(\Gamma_{out})$ is a consistent boundary condition if $\overline{g}_{out}(x,y) = \overline{g}_{in}(x,y)$.*

5.2. Uniqueness. Now we want to prove the equivalence between problem (5.18) and

$$\begin{cases} \dfrac{-\nabla u(x,y)\cdot\widetilde{\omega}' + \omega_3'}{\sqrt{1+|\nabla u(x,y)|^2}} = I_1(x,y) & \text{a.e. } (x,y)\in\Omega, \\ \dfrac{-\nabla u(x,y)\cdot\widetilde{\omega}'' + \omega_3''}{\sqrt{1+|\nabla u(x,y)|^2}} = I_2(x,y) & \text{a.e. } (x,y)\in\Omega, \\ u(x,y) = g(x,y) & \forall (x,y)\in\partial\Omega. \end{cases} \tag{5.44}$$

Proposition 5.6. *If $v(x,y)$ is a solution of the nonlinear system (5.44), then it is also a solution of (5.18).*

Proof. We will prove that the two problems are equivalent in the physical case, that is, when we consider the relation between the two images and the surface:

$$\begin{cases} I_1(x,y) = G_{\omega'}(v) = \dfrac{-\nabla v(x,y)\cdot\widetilde{\omega}' + \omega_3'}{\sqrt{1+|\nabla v(x,y)|^2}}, & (x,y)\in\Omega, \\ I_2(x,y) = G_{\omega''}(v) = \dfrac{-\nabla v(x,y)\cdot\widetilde{\omega}'' + \omega_3''}{\sqrt{1+|\nabla v(x,y)|^2}}, & (x,y)\in\Omega. \end{cases} \tag{5.45}$$

Let us call $G_{\omega'}(v)$ and $G_{\omega''}(v)$ the operators that describe the SfS classical problem applied to the surface v. We now want to emphasize how the functions $I_1(x,y)$, $I_2(x,y)$ and the function u, solution of problem (5.18), are correlated. First, we fix the light sources, so the applications $G_{\omega'}(v)$ and $G_{\omega''}(v)$ are univocally determined (that is, if we assign a surface v, it is always possible to calculate the brightness images I_1 and I_2, respectively, for the light vectors ω' and ω''), but they are not bijective (because it's not possible to determine the surface v only by the single function of the brightness and the value of the surface on the boundary of the set Ω). Now we want to verify that, if u satisfies (5.18) and we add the condition $u(x,y) = v(x,y)$ for the $(x,y) \in \partial\Omega$, then $u(x,y) = v(x,y)$ in Ω. If we consider v as the solution of the nonlinear system, we can use the fact that it generates the image functions I_1 and I_2. Then, by substitution we have

$$\nabla u(x,y)\cdot(\widetilde{\omega}' G_{\omega''}(v) - \widetilde{\omega}'' G_{\omega'}(v)) = \omega_3' G_{\omega''}(v) - \omega_3'' G_{\omega'}(v); \tag{5.46}$$

then

$$\nabla u(x,y)\cdot\left(\widetilde{\omega}'\frac{-\nabla v(x,y)\cdot\widetilde{\omega}''+\omega_3''}{\sqrt{1+|\nabla v(x,y)|^2}}-\widetilde{\omega}''\frac{-\nabla v(x,y)\cdot\widetilde{\omega}'+\omega_3'}{\sqrt{1+|\nabla v(x,y)|^2}}\right)$$
$$=\omega_3'\frac{-\nabla v(x,y)\cdot\widetilde{\omega}''+\omega_3''}{\sqrt{1+|\nabla v(x,y)|^2}}-\omega_3''\frac{-\nabla v(x,y)\cdot\widetilde{\omega}'+\omega_3'}{\sqrt{1+|\nabla v(x,y)|^2}},$$

$$\nabla u(x,y)\cdot((-\nabla v(x,y)\cdot\widetilde{\omega}'')\widetilde{\omega}'+\omega_3''\widetilde{\omega}'+(\nabla v(x,y)\cdot\widetilde{\omega}')\widetilde{\omega}''-\omega_3'\widetilde{\omega}'')$$
$$=-\nabla v(x,y)\cdot\widetilde{\omega}''\omega_3'+\omega_3'\omega_3''+\nabla v(x,y)\cdot\widetilde{\omega}'\omega_3''-\omega_3'\omega_3'',$$

$$\nabla u(x,y)\cdot((-\nabla v(x,y)\cdot\widetilde{\omega}'+\nabla v(x,y)\cdot\widetilde{\omega}')\widetilde{\omega}''+\omega_3''\widetilde{\omega}'-\omega_3'\widetilde{\omega}'')=-\nabla v(x,y)\cdot(\widetilde{\omega}''\omega_3'-\widetilde{\omega}'\omega_3''),$$

for which

$$\nabla u(x,y)\cdot(\omega_3''\widetilde{\omega}'-\omega_3'\widetilde{\omega}'')=\nabla v(x,y)\cdot(\widetilde{\omega}'\omega_3''-\widetilde{\omega}''\omega_3'),$$

and this implies the equality $\nabla u(x,y)=\nabla v(x,y)$ in Ω. If we consider the condition $u(x,y)=v(x,y)$ for the points $(x,y)\in\partial\Omega$, we obtain the extension of the equality also in all the domain. ■

We will use now this result for the uniqueness of solution of problem (5.44), as follows.

Corollary 5.7. *The nonlinear system* (5.44) *admits only one solution.*

Proof. If, by contradiction, we take two solutions of problem (5.44) called $v_1(x,y)$ and $v_2(x,y)$, then, by (5.6) we can also say that both are solutions of problem (5.18). However, by the uniqueness result Theorem 5.3, this implies $v_1(x,y)=v_2(x,y)$ for any $(x,y)\in\Omega$. ■

6. Some approximation schemes for the SfS-PS linear equation. We have seen how the system of nonlinear equations can be transformed into a stationary linear equation. In this section we are going to present some numerical schemes to compute the weak solution of the problem.

For simplicity, let us consider a square domain Ω like the set $[a,b]^2$ (in the numerical tests $[a,b]=[-1,1]$) and with a uniform discretization space step $\Delta=(b-a)/n$, where n is the number of intervals dividing the side of the square. Then we have $x_i=a+i\Delta$, $y_j=a+j\Delta$ with $i,j=0,\ldots,n$. We will denote by $\overline{\Omega}_d$ all the points of the lattice belonging to $\overline{\Omega}$, by Ω_d all the internal points, and by $\partial\Omega_d$ all the boundary points.

6.1. Finite difference. We start with a standard finite difference approximation of the partial derivatives of u:

$$\frac{\partial u}{\partial x}(x_i,y_j)=\frac{u(x_{i+1},y_{j+1})-u(x_{i-1},y_{j+1})}{2\Delta}+\mathcal{O}(\Delta^2)\quad\text{(central)},$$

$$\frac{\partial u}{\partial y}(x_i,y_j)=\frac{u(x_i,y_{j+1})-u(x_i,y_j)}{\Delta}+\mathcal{O}(\Delta)\quad\text{(right)}.$$

Note that even if we use the implicit finite difference schemes (usually used to ameliorate the stability of this kind of technique), we must respect some constraints to guarantee convergence [46].

Starting with knowledge of the solution on part of the boundary, we use the two above approximations to build the following implicit scheme for (4.8):

$$U(x_i,y_{j+1})+\frac{b_1(x_i,y_{j+1})}{2b_2(x_i,y_j)}(U(x_{i+1},y_{j+1})-U(x_{i-1},y_{j+1})) = U(x_i,y_j)+\frac{\Delta}{b_2(x_i,y_j)}f(x_i,y_j). \tag{6.1}$$

In particular we will use the values at the left, right, and lower sides of the domain as boundary conditions. Since we divide by the second component of the vector field b, it is clear that the numerical scheme is not defined at every point (x_i,y_j) such that $b_2(x_i,y_j)=0$ (note that situation can appear even if $|b|\neq 0$).

Then, for every line of the domain (and for $j=0,\dots,n-1$) we have to solve the linear system

$$AU_{j+1}=B,$$

where the unknown vector that contains all the values of U in the $(j+1)$th row and the right-hand side can be written as

$$U_{j+1}=\begin{pmatrix} U_{1,j+1}\\ U_{2,j+1}\\ \vdots\\ \vdots\\ U_{n-2,j+1}\\ U_{n-1,j+1}\end{pmatrix},\quad B=\begin{pmatrix} U_{1,j}+\frac{\Delta}{b^2_{1,j}}f_{1,j}+\frac{b^1_{1,j+1}}{2b^2_{1,j}}U_{0,j+1}\\ U_{2,j}+\frac{\Delta}{b^2_{2,j}}f_{2,j}\\ \vdots\\ \vdots\\ U_{n-2,j}+\frac{\Delta}{b^2_{n-2,j}}f_{n-2,j}\\ U_{n-1,j}+\frac{\Delta}{b^2_{n-1,j}}f_{n-1,j}-\frac{b^1_{n,j+1}}{2b^2_{n,j}}U_{n,j+1}\end{pmatrix}, \tag{6.2}$$

and $b^1_{i,j}=b_1(x_i,y_j)$ and $b^2_{i,j}=b_2(x_i,y_j)$. It is important to remark that the matrix A of the coefficients is tridiagonal:

$$A=\begin{pmatrix} 1 & \frac{b^1_{1,j+1}}{2b^2_{1,j}} & 0 & 0 & \dots & 0\\ -\frac{b^1_{2,j+1}}{2b^2_{2,j}} & 1 & \frac{b^1_{2,j+1}}{2b^2_{2,j}} & 0 & \dots & 0\\ 0 & \ddots & \ddots & \ddots & \ddots & \vdots\\ \vdots & \ddots & \ddots & \ddots & \ddots & 0\\ 0 & \dots & 0 & -\frac{b^1_{n-2,j+1}}{2b^2_{n-2,j}} & 1 & \frac{b^1_{n-2,j+1}}{2b^2_{n-2,j}}\\ 0 & \dots & \dots & 0 & -\frac{b^1_{n-1,j+1}}{2b^2_{n-1,j}} & 1\end{pmatrix}. \tag{6.3}$$

Let us analyze the stability of this scheme via the classical von Neumann analysis. If we prove the stability for this scheme, we can use the principle of Duhamel (see [43]), which states that the scheme for the inhomogeneous problem is stable if the corresponding scheme for the homogeneous scheme is stable.

To this end, take the homogeneous differential equation

$$b(x,y)\cdot\nabla u(x,y)=0, \tag{6.4}$$

and consider the following implicit scheme:

$$U(x_i,y_{j+1})+\frac{b_1(x_i,y_{j+1})}{2b_2(x_i,y_j)}(U(x_{i+1},y_{j+1})-U(x_{i-1},y_{j+1}))=U(x_i,y_j) \tag{6.5}$$

with $u(x_0,y_j)$, $u(x_n,y_j)$, and $u(x_i,y_0)$ given for $i,j=0,\dots,n$.

Let $u(x_i,y_j)$ be the continuous solution of the finite difference scheme (6.5) and $U(x_i,y_j)$ the solution of the scheme which is computed, so that $U(x_i,y_j)$ contains rounding errors. The error at every mesh point (x_i,y_j) is defined as

$$E(x_i,y_j)=u(x_i,y_j)-U(x_i,y_j).$$

Assume that the solution is periodic. Substituting into the scheme the solution developed in Fourier series, we get

$$E(x_i,y_j)=e^{\alpha j\Delta}e^{\mathbf{i}\beta i\Delta}, \tag{6.6}$$

where $\mathbf{i}^2$ denotes the imaginary unit; then a finite difference scheme with constant coefficients is stable if

$$|e^{\alpha\Delta}|\le 1\quad\forall\alpha\in\mathbb{R}. \tag{6.7}$$

Theorem 6.1. *The numerical scheme* (6.5) *is unconditionally stable.*

Proof. We have to show that condition (6.7) is satisfied. Taking the scheme (6.5) we have

$$e^{\alpha(j+1)\Delta}e^{I\beta i\Delta}+\frac{\overline{b}}{2}\big(e^{\alpha(j+1)\Delta}e^{\mathbf{i}\beta(i+1)\Delta}-e^{\alpha(j+1)\Delta}e^{\mathbf{i}\beta(i-1)\Delta}\big)=e^{\alpha j\Delta}e^{\mathbf{i}\beta i\Delta},$$

where $\overline{b}=\max_{(x_i,y_j)\in\Omega_d}\frac{b_1(x_i,y_{j+1})}{b_2(x_i,y_j)}$. Dividing by $e^{\alpha(j+1)\Delta}e^{\mathbf{i}\beta i\Delta}$ yields

$$1+\frac{\overline{b}}{2}\big(e^{\mathbf{i}\beta\Delta}-e^{-\mathbf{i}\beta\Delta}\big)=e^{-\alpha\Delta},$$

$$1+\frac{\overline{b}}{2}(2\mathbf{i}\sin(\beta\Delta))=e^{-\alpha\Delta};$$

then

$$e^{-\alpha\Delta}=\frac{1-\overline{b}\mathbf{i}\sin(\beta\Delta)}{1+\overline{b}^2\sin^2(\beta\Delta)}<1. \qquad \blacksquare$$

However, even if the stability can be reached, if there exists a point (x_i,y_j) such that $b_2(x_i,y_j)=0$, the discretized problem (6.3) cannot be solved.

6.1.1. Forward upwind scheme. In order to introduce a finite difference numerical scheme which does not need to consider a particular direction of the vector field b in order to be well defined, let us consider the following implicit upwind scheme:

$$b^1_{i,j}\frac{U^F_{i+1,j}-U^F_{i-1,j}}{2\Delta}+b^2_{i,j}\frac{U^F_{i,j+1}-U^F_{i,j-1}}{2\Delta} = |b^1_{i,j}|\frac{U^F_{i+1,j}-2U^F_{i,j}+U^F_{i-1,j}}{2\Delta}+|b^2_{i,j}|\frac{U^F_{i,j+1}-2U^F_{i,j}+U^F_{i,j-1}}{2\Delta}+f_{i,j} \tag{6.8}$$

for $i,j=1,\dots,n-1$. The artificial diffusion introduced in the right-hand side of (6.8) produces the upwind correction for the vector field b, taking the forward or backward discretization for the first derivatives in order to follow the characteristic lines [36, 43]. In particular, the numerical scheme is consistent of order 1 with respect to both partial derivatives.

Now the computation of U^F can be obtained via a global linear system where all the internal points of the grid are included. This means that the dimension of the system is of $[(n-1)(n-1)]\times[(n-1)(n-1)]$. Note that a priori the corresponding matrix has a block structure. In fact, writing the scheme (6.8) as

$$\begin{aligned} &U^F_{i+1,j}\left(\frac{b^1_{i,j}-|b^1_{i,j}|}{2\Delta}\right)-U^F_{i-1,j}\left(\frac{b^1_{i,j}+|b^1_{i,j}|}{2\Delta}\right)+U^F_{i,j}\left(\frac{|b^1_{i,j}|+|b^2_{i,j}|}{\Delta}\right)\\ &+U^F_{i,j+1}\left(\frac{b^2_{i,j}-|b^2_{i,j}|}{2\Delta}\right)-U^F_{i,j-1}\left(\frac{b^2_{i,j}+|b^2_{i,j}|}{2\Delta}\right)=f_{i,j}, \end{aligned} \tag{6.9}$$

we obtain the block linear system

$$\begin{pmatrix} D^F_1 & D^{S_F}_1 & 0 & \dots & \dots & \dots & 0\\ D^{I_F}_1 & D^F_2 & D^{S_F}_2 & 0 & \dots & \dots & 0\\ 0 & D^{I_F}_2 & D^F_3 & D^{S_F}_3 & 0 & \dots & 0\\ \vdots & \ddots & \ddots & \ddots & \ddots & \ddots & \vdots\\ 0 & \dots & 0 & D^{I_F}_{n-4} & D^F_{n-3} & D^{S_F}_{n-3} & 0\\ 0 & \dots & \dots & 0 & D^{I_F}_{n-3} & D^F_{n-2} & D^{S_F}_{n-2}\\ 0 & \dots & \dots & \dots & 0 & D^{I_F}_{n-2} & D^F_{n-1} \end{pmatrix} \begin{pmatrix} U^F_{\text{bloc}_1}\\ U^F_{\text{bloc}_2}\\ U^F_{\text{bloc}_3}\\ \vdots\\ U^F_{\text{bloc}_{n-3}}\\ U^F_{\text{bloc}_{n-2}}\\ U^F_{\text{bloc}_{n-1}} \end{pmatrix} = \begin{pmatrix} B^F_{\text{bloc}_1}\\ B^F_{\text{bloc}_2}\\ B^F_{\text{bloc}_3}\\ \vdots\\ B^F_{\text{bloc}_{n-3}}\\ B^F_{\text{bloc}_{n-2}}\\ B^F_{\text{bloc}_{n-1}} \end{pmatrix}, \tag{6.10}$$

where D^F_r, $D^{S_F}_k$, $D^{I_F}_k$ are matrices of $\mathbb{R}^{(n-1)\times(n-1)}$ and $U^F_{\text{bloc}_r}$, $b^F_{\text{bloc}_r}$ are vectors of $\mathbb{R}^{n-1}$ (with $r=1,\dots,n-1$ and $k=1,\dots,n-2$). In particular,

$$D^F_r=\begin{pmatrix} \frac{|b^1_{1,r}|+|b^2_{1,r}|}{\Delta} & \frac{b^1_{1,r}-|b^1_{1,r}|}{2\Delta} & 0 & \dots & \dots & 0\\ -\frac{b^1_{2,r}+|b^1_{2,r}|}{2\Delta} & \frac{|b^1_{2,r}|+|b^2_{2,r}|}{\Delta} & \frac{b^1_{2,r}-|b^1_{2,r}|}{2\Delta} & 0 & \dots & 0\\ 0 & \ddots & \ddots & \ddots & \ddots & 0\\ 0 & \dots & 0 & -\frac{b^1_{n-2,r}+|b^1_{n-2,r}|}{2\Delta} & \frac{|b^1_{n-2,r}|+|b^2_{n-2,r}|}{\Delta} & \frac{b^1_{n-2,r}-|b^1_{n-2,r}|}{2\Delta}\\ 0 & \dots & \dots & 0 & -\frac{b^1_{n-1,r}+|b^1_{n-1,r}|}{2\Delta} & \frac{|b^1_{n-1,r}|+|b^2_{n-1,r}|}{\Delta} \end{pmatrix},$$

$$D^{S_F}_k=\operatorname{diag}\left(\frac{b^2_{1,k}-|b^2_{1,k}|}{2\Delta},\frac{b^2_{2,k}-|b^2_{2,k}|}{2\Delta},\dots,\frac{b^2_{n-2,k}-|b^2_{n-2,k}|}{2\Delta},\frac{b^2_{n-1,k}-|b^2_{n-1,k}|}{2\Delta}\right),$$

$$D_k^{I_F} = \operatorname{diag}\left(-\frac{b^2_{1,k+1}+|b^2_{1,k+1}|}{2\Delta}, -\frac{b^2_{2,k+1}+|b^2_{2,k+1}|}{2\Delta}, \dots, -\frac{b^2_{n-2,k+1}+|b^2_{n-2,k+1}|}{2\Delta}, -\frac{b^2_{n-1,k+1}+|b^2_{n-1,k+1}|}{2\Delta} \right),$$

$$B^F_{\text{bloc}_1} = \begin{pmatrix} u_{1,0}\frac{b^2_{1,1}+|b^2_{1,1}|}{2\Delta} + u_{0,1}\frac{b^1_{1,1}+|b^1_{1,1}|}{2\Delta} + f_{1,1} \\ u_{2,0}\frac{b^2_{2,1}+|b^2_{2,1}|}{2\Delta} + f_{2,1} \\ \vdots \\ u_{n-2,0}\frac{b^2_{n-2,1}+|b^2_{n-2,1}|}{2\Delta} + f_{n-2,1} \\ u_{n-1,0}\frac{b^2_{n-1,1}+|b^2_{n-1,1}|}{2\Delta} - u_{n,1}\frac{b^1_{n-1,1}-|b^1_{n-1,1}|}{2\Delta} + f_{n-1,1} \end{pmatrix},$$

$$B^F_{\text{bloc}_q} = \begin{pmatrix} u_{0,q}\frac{b^1_{1,q}+|b^1_{1,q}|}{2\Delta} + f_{1,q} \\ f_{2,q} \\ \vdots \\ f_{n-2,q} \\ -u_{n,q}\frac{b^1_{n-1,q}-|b^1_{n-1,q}|}{2\Delta} + f_{n-1,q} \end{pmatrix} \qquad \text{for } q = 2, \dots, n-2,$$

$$B^F_{\text{bloc}_{n-1}} = \begin{pmatrix} -u_{1,n}\frac{b^2_{1,n-1}-|b^2_{1,n-1}|}{2\Delta} + u_{0,n-1}\frac{b^1_{1,n-1}+|b^1_{1,n-1}|}{2\Delta} + f_{1,n-1} \\ -u_{2,n}\frac{b^2_{2,n-1}-|b^2_{2,n-1}|}{2\Delta} + f_{2,n-1} \\ \vdots \\ -u_{n-2,n}\frac{b^2_{n-2,n-1}-|b^2_{n-2,n-1}|}{2\Delta} + f_{n-2,n-1} \\ -u_{n-1,n}\frac{b^2_{n-1,n-1}-|b^2_{n-1,n-1}|}{2\Delta} - u_{n,n-1}\frac{b^1_{n-1,n-1}-|b^1_{n-1,n-1}|}{2\Delta} + f_{n-1,n-1} \end{pmatrix},$$

and

$$U^F_{bloc_r} = (U^F_{1,r}, \dots, U^F_{n-1,r}) \qquad \text{for } r = 1, \dots, n-1. \tag{6.11}$$

After this global description of the discretization matrix is it important to emphasize the local structure of the matrix. It is clear that it depends on the vector field b. In fact, we note that a lot of coefficients in the previous matrices are zero. That is, if we consider the two quantities

$$-\frac{b^1_{i,j}+|b^1_{i,j}|}{2\Delta}, \qquad \frac{b^1_{i,j}-|b^1_{i,j}|}{2\Delta},$$

only one can be different from zero, depending on the sign of $b^1_{i,j}$. The same argument is true for the other coefficients far away from the diagonal:

$$-\frac{b^2_{i,j}+|b^2_{i,j}|}{2\Delta}, \qquad \frac{b^2_{i,j}-|b^2_{i,j}|}{2\Delta}.$$

The above remark shows that the matrix appearing in system (6.10) may also have zero elements on the five diagonals. This way of discretizing problem (5.18) allows us to approximate the solution by considering the inflow part of the image boundary (i.e., $g_{in}(x, y)$) since

we follow the characteristics which propagate the information at the boundary across the domain. In Appendix A.2 we describe how it is possible to compute the unique solution of problem (5.18) starting from the other side of the boundary (namely, the backward upwind scheme), that is, Γ_{out}, considering as initial boundary data $g_{out}(x, y)$.

6.2. A forward semi-Lagrangian discretization. A second numerical approach to solving (5.18) is to mimic the solution along the characteristics in the general case, i.e., when they are not parallel to the axis as in the finite difference case. We then consider the following equivalent equation obtained by dividing the two sides of (5.18) by the norm of $b(x, y)$:

$$\nabla_\rho u(x, y) = \frac{f(x, y)}{|b(x, y)|} \quad \forall (x, y) \in \Omega, \tag{6.12}$$

where $\nabla_\rho u$ denotes the directional derivative of u in the direction $\rho(x, y) = \frac{b(x,y)}{|b(x,y)|}$.

We observe that the division by $|b(x, y)|$ doesn't involve any kind of difficulties for the numerical scheme, due to Lemma 5.1. Now, considering the definition of directional derivative, we can write

$$\lim_{h\to 0} -\frac{u(x - h\rho_1(x, y), y - h\rho_2(x, y)) - u(x, y)}{h} = \frac{f(x, y)}{|b(x, y)|} \quad \forall (x, y) \in \Omega, \tag{6.13}$$

which leads to the approximation

$$-\frac{u(x - h\rho_1(x, y), y - h\rho_2(x, y)) - u(x, y)}{h} \simeq \frac{f(x, y)}{|b(x, y)|} \quad \forall (x, y) \in \Omega. \tag{6.14}$$

Considering a uniform discretization $\overline{\Omega}_d$ as in the previous section, we can finally write the semi-Lagrangian scheme

$$u(x_i, y_j) = u(x_i - h\rho_1(x_i, y_j), y_j - h\rho_2(x_i, y_j)) + \frac{f(x_i, y_j)}{|b(x_i, y_j)|} h. \tag{6.15}$$

This scheme has the advantage of following a numerical integration along the characteristics of (5.18), but it has some computational drawbacks:

- it computes for every point $(x_i, y_j) \in \Omega_d$ a linear system for the interpolation of the point $u(x_i - h\rho_1(x_i, y_j), y_j - h\rho_2(x_i, y_j))$ with respect to the (uniform) grid;
- it is an iterative method since it is based on a fixed point scheme.

We introduce two discrete functions $u^n(x_i, y_j) = u^n_{i,j}$ and $u^{n+1}(x_i, y_j) = u^{n+1}_{i,j}$ defined only on the grid nodes. Therefore, the iterative scheme (6.15) corresponds to

$$u^{n+1}_{i,j} = u^n(x_i - h\rho_1(x_i, y_j), y_j - h\rho_2(x_i, y_j)) + \frac{f_{i,j}}{|b_{i,j}|} h \quad \forall (x_i, y_j) \in \Omega_d. \tag{6.16}$$

If we assign an initial function $u^0_{i,j}$, such that $u^0(x_i, y_j) = g(x_i, y_j)$ for any $l(x_i, y_j) \in \partial\Omega_d$, it is possible to start the iterations by computing the successive approximation $u^{n+1}_{i,j}$ as in (6.16).

This numerical scheme works by following the direction of the characteristics. This means that it will need the boundary data on the inflow part of $\partial\Omega$ (i.e., Γ_{in}). As explained in the previous section, also for the semi-Lagrangian scheme it is possible to approximate the solution using the other part of the boundary condition (that is, $g_{out}(x, y)$); see Appendix A.1.

6.2.1. Consistency and convergence. In this section we want to prove the convergence of the semi-Lagrangian numerical schemes, given as known the construction of the bilinear interpolation and the order of consistency [14]. In fact, for both schemes (backward and forward) we have the following order of consistency:

$$\mathcal{O}(h) + \mathcal{O}\left(\frac{\Delta^2}{h}\right) \tag{6.17}$$

for which we can obtain order one of consistency if we take $h = \Delta$.

Let us now give a proof of the convergence of this method. In this case we will show that the numerical algorithm is a nonincreasing map in $L^\infty(\Omega)$ on the Banach space function $W^{1,\infty}(\Omega)$, that is, the Sobolev space notation for the Lipschitz-type functions.

In order to prove the convergence of the scheme using the existence of a unique fixed point for the nonexpansive map [21], we give the following definition.

Definition 6.2 (condition A). *If D is a subset of a Banach space X, T is a mapping from D into X, and $x_1 \in D$, then $M(x_1, t_n, T)$ is the sequence $\{x_n\}_{n=1}^\infty$ defined by $x_{n+1} = (1 - t_n)x_n + t_n T x_n$, where $\{t_n\}_{n=1}^\infty$ is a real sequence. If a point x_1 and a sequence $\{t_n\}_{n=1}^\infty$ satisfy the three conditions*

$$\sum_{n=1}^{\infty} t_n = \infty, \tag{6.18}$$

$$0 \le t_n \le b < 1 \qquad \forall \text{ positive integers } n, \tag{6.19}$$

then x_1 and $\{t_n\}_{n=1}^\infty$ will be said to satisfy condition A.

Note that if $t_n \in [a, b]$ for all positive integers n and $0 < a \le b < 1$, then it is obvious that the sequence $\{t_n\}_{n=1}^\infty$ satisfies (6.18) and (6.19).

Theorem 6.3. *Let D be a closed subset of a Banach space X, and let $T : D \to X$ be a nonexpansive mapping with X compact. If there exist x_1 and $\{t_n\}_{n=1}^\infty$ that satisfy condition A, then T has a fixed point in D and $M(x_1, t_n, T)$ converges to a fixed point of T.*

Using the previous result, we want to prove the convergence of the numerical semi-Lagrangian schemes using the fact that the operator that defines the schemes satisfies condition A.

Theorem 6.4. *The numerical scheme (6.16) (and (A.2)) converges to the unique weak solution of problem (5.18).*

Proof. First we define the map T described by the numerical scheme (6.16) on the Lipschitz functional space:

$$T(u)(x, y) = u((x, y) + h\rho(x, y)) - h\frac{f(x, y)}{|b(x, y)|}. \tag{6.20}$$

It is easy to see that (6.20) is nonexpansive in $W^{1,\infty}(\Omega)$. In fact, if we take two functions u and w both in $W^{1,\infty}(\Omega)$, then

$$\begin{aligned} &\|T(u)(x, y) - T(w)(x, y)\|_\infty \\ &= \left\| u((x, y) + h\rho(x, y)) - h\frac{f(x, y)}{|b(x, y)|} - w((x, y) + h\rho(x, y)) + h\frac{f(x, y)}{|b(x, y)|} \right\|_\infty \\ &= \|u((x, y) + h\rho(x, y)) - w((x, y) + h\rho(x, y))\|_\infty = \|u(x, y) - w(x, y)\|_\infty. \end{aligned}$$

The iterative method uses this map to build the sequence by the recursive scheme, that is, $u^{n+1} = T(u^n)$. In order to use the previous theorem we define some objects useful to this purpose. Let $M(v^0, t_n, T)$ be the sequence defined as

$$v^{n+1} = (1 - t_n)v^n + t_n T(v^n), \tag{6.21}$$

where $v^0 \in W^{1,\infty}(\Omega)$ is the initial data and $\{t_n\}_{n=0}^{\infty}$ is a sequence of real numbers such that

$$\sum_{n=0}^{\infty} t_n = \infty \quad \text{with } 0 \leq t_n \leq b < 1,$$

with $b \in \mathbb{R}$. In our case it is also possible to take t_n as a constant sequence (for example, $t_n = \frac{1}{2}$ would be enough).

In the weakest case (where we prove the existence and the uniqueness, Theorem 5.3), we consider that the functions $b(x, y)$ and $f(x, y)$ are discontinuous on the same curve $\gamma(t) \subset \Omega$. The operator T is applied on functions taken in a discrete domain Ω_d. Then if we consider $\frac{f(x,y)}{|b(x,y)|}$ with $(x, y) \in \Omega_d$ as the values of a function in $W^{1,\infty}(\Omega)$, the following can be considered true:

$$v^n \in W^{1,\infty}(\Omega) \quad \forall n \geq 0.$$

We finally have all the necessary hypotheses satisfied in order to apply the previous theorem, Theorem 6.3. ■

The computational cost for every iteration of both schemes is considerable, taking into account that for every internal point of the grid we have to solve a linear system whose dimension is small and constant for every point. Since in the numerical tests we use a bilinear interpolation, at every pixel we solve a linear system of dimension four.

The stopping criterion is based on the convergence of the succession of approximations u^n through the Cauchy criterion with the infinity norm; that is, since u^n converges to u, the algorithm will be stopped when

$$||u^n - u^{n+1}||_\infty := \max_{(x_i,y_j)\in\Omega_d} |u^n(x_i, y_j) - u^{n+1}(x_i, y_j)| < \varepsilon \tag{6.22}$$

with ε opportunely chosen small.

7. Numerical tests.

In this section we will test the semi-Lagrangian and the upwind finite difference scheme (forward and backward) on a set of surfaces. In order to prove the efficiency of the model previously described, we use both synthetic and real images, and also consider regular and Lipschitz continuous surfaces.

7.1. Synthetic images.

The different types of surfaces represented in Figure 9 have been chosen because their geometrical and analytical properties have an impact on the convergence of the schemes. In particular, $v_1(x, y)$ is a regular surface with three peaks corresponding to very big slopes. In order to verify that the numerical schemes converge even if some theoretical assumptions with respect to Theorem 5.3 are not verified, we use the surface $v_2(x, y)$, which has an easy disposition of the point of nondifferentiability of the surface. We will see that it is possible to choose the field b in order to have some curves of nondifferentiability coincident

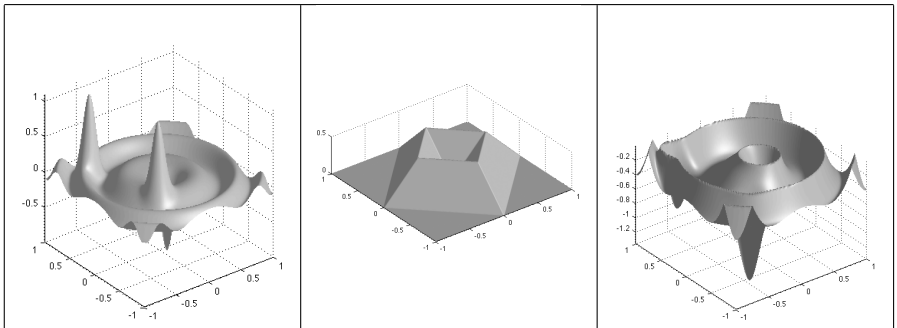

$v_1(x,y)$	$v_2(x,y)$	$v_3(x,y)$
[-0.989,1.088]	[0.0,0.5]	[-1.365,0.0]

Figure 9. *Benchmark surfaces used for the numerical tests with the respective range of values (below).*

with the characteristic curves. The last surface $v_3(x,y)$ still is a.e. differentiable like the previous one, but it does has not have a regular structure. In particular we can see that the boundary is also not differentiable everywhere.

For our numerical tests we consider two light sources expressed in the spherical coordinates $(\omega = (\sin(\varphi)\cos(\theta), \sin(\theta)\sin(\varphi), \cos(\varphi)))$ in order to avoid black shadows using (2.1). As explained in section 4, this new differential approach can work also with a variable albedo. In this numerical test we will consider a uniform albedo (equal to 1). The size of the images taken into account varies from 100×100 pixels (with $\Delta = 0.02$) to 800×800 pixels (for a spatial step $\Delta = 0.0025$).

For the semi-Lagrangian scheme we start with the iterations of (6.16) and (A.2) until condition (6.22) is satisfied. We choose $h = \Delta$ to obtain the best convergence order. The linear system obtained from the upwind schemes is solved using the Gauss–Seidel method since the matrix of discretization (6.10) is diagonally dominant.

Once we construct the images (see Figure 10, 12, and 11) from the analytical formula of the surface (namely $v(x,y)$), we compute the initial guess, for both methods, such that $u^0(x_i,y_j) = v(x_i,y_j)$ for all (x_i,y_j) in $\partial\Omega_d$ and $u^0 = 0$ in Ω_d. We use a parameter $\varepsilon = 10^{-7}$ for the convergence of the iterative methods and, denoting by $\overline{n}$ the index of the last iteration, the error in the $L^\infty(\Omega_d)$ norm appearing in Tables 1–4 is defined as

$$E = \max_{(x_i,y_j)\in\Omega_d} |u^{\overline{n}}(x_i,y_j) - v(x_i,y_j)|.$$

Test 1. Here we show how the numerical schemes work on smooth surfaces having rather high gradients. The starting images are shown in Figure 10 with the respective light sources written in polar coordinates.

In Table 1 the errors in the $L^\infty(\Omega_d)$ norm are written for each numerical scheme, and the order of convergence is indicated. We note that the upwind schemes are faster than the semi-Lagrangian schemes, but are less accurate. Moreover, even if the regularity of the surface should preserve the theoretical order (i.e., 1), the numerical order of convergence is lower than 1.

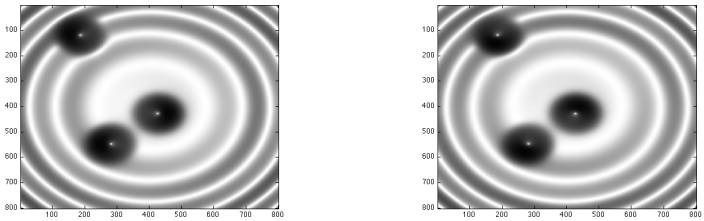

Test 1. I_1 has $\omega' : \varphi_1 = 0.1, \theta_1 = 0.$ I_2 has $\omega'' : \varphi_2 = 0.1, \theta_2 = \frac{7}{18}\pi.$

Figure 10. *Benchmark images and their light sources (in spherical coordinates). These initial data have been used in the numerical tests in Table 1.*

Table 1

Error in $L^\infty(\Omega_d)$ norm and order of convergence relative to v_1.

Δ	SL-F error	SL-F order	UW-F	UW-F order
0.02	1.985×10^{-1}		2.115×10^{-1}	
0.01	9.754×10^{-2}	1.025	1.212×10^{-1}	0.811
0.005	4.788×10^{-2}	1.026	6.812×10^{-2}	0.835
0.0025	2.376×10^{-2}	1.010	3.685×10^{-2}	0.889
Δ	SL-B error	SL-B order	UW-B	UW-B order
0.02	1.985×10^{-1}		2.031×10^{-1}	
0.01	9.754×10^{-2}	1.025	1.088×10^{-1}	0.903
0.005	4.788×10^{-2}	1.026	5.628×10^{-2}	0.951
0.0025	2.376×10^{-2}	1.010	2.866×10^{-2}	0.973

Test 2. The surface v_2 has been chosen to analyze how the curves where the images I_1 and I_2 are discontinuous (shown in blue in Figure 11) can influence the convergence of the numerical schemes.

Let us consider this surface for a first set of starting data (images and respective light sources are shown in Figure 11) in order to see that the discontinuity curves do not block the convergence of the numerical schemes. Note that the order is 1.

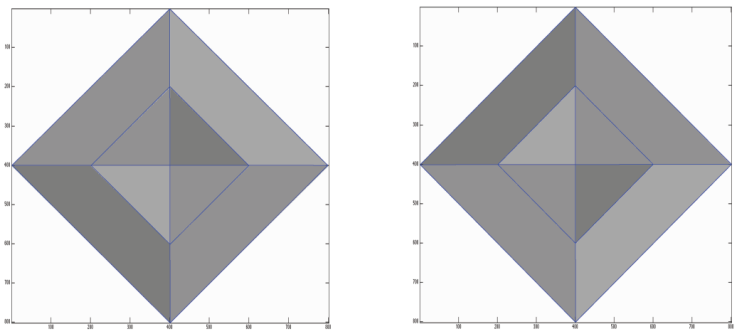

Test 2. I_1 for $\omega' : \varphi_1 = 0.1, \theta_1 = \frac{\pi}{4}.$ I_2 for $\omega'' : \varphi_2 = 0.1, \theta_2 = \frac{7}{4}\pi.$

Figure 11. *Benchmark images and their light sources (in spherical coordinates). These initial data have been used in the numerical tests in Table 2. For each surface it is possible to see the curve where the surface is not differentiable (in blue).*

From Table 2 we can see that the semi-Lagrangian schemes have smaller errors than the upwind ones. It is also possible to see the better convergence of the semi-Lagrangian approximations looking at the order of convergence.

Table 2

Error in $L^\infty(\Omega_d)$ norm and order of convergence relative to v_2.

Δ	SL-F error	SL-F order	UW-F	UW-F order
0.02	3.829×10^{-2}		2.808×10^{-2}	
0.01	1.919×10^{-2}	0.996	1.483×10^{-2}	0.921
0.005	9.930×10^{-3}	0.950	7.880×10^{-3}	0.913
0.0025	5.020×10^{-3}	0.984	4.180×10^{-3}	0.913
Δ	SL-B error	SL-B order	UW-B	UW-B order
0.02	3.678×10^{-2}		2.808×10^{-2}	
0.01	1.872×10^{-2}	0.974	1.483×10^{-2}	0.921
0.005	9.390×10^{-3}	0.995	7.880×10^{-3}	0.913
0.0025	7.540×10^{-3}	0.998	4.180×10^{-3}	0.913

Test 3. This test uses v_3 and is intended to show that surfaces with a high Lipschitz constant can cause trouble in the approximation. In this case the curves where the surface is not differentiable (shown in blue in Figure 12) are not straight lines as in the previous case. This aspect influences the approximation and the convergence of the numerical schemes used.

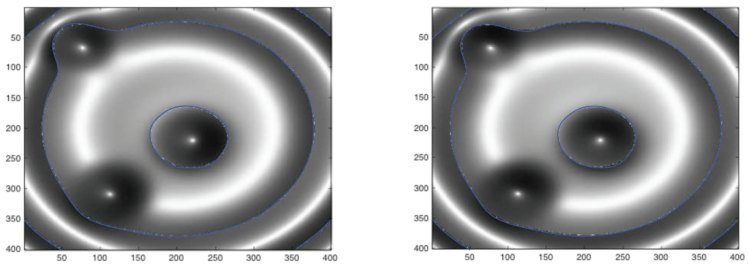

Test 3. I_1 for $\omega' : \varphi_1 = 0.1, \theta_1 = 0$. I_2 for $\omega'' : \varphi_2 = 0.1, \theta_2 = \frac{7}{18}\pi$.

Figure 12. *Benchmark images and their light sources (in spherical coordinates). These initial data have been used in the numerical tests in Table 3. It is possible to see the curve where the surface is not differentiable (in blue).*

In Table 3 we can see the convergence of all the numerical schemes although the order is not close to the theoretical one. With the aim of understanding how the order is influenced by these curves, we will consider a particular configuration of the vector field with respect to the surface v_2.

Test 4. Since for Table 3 we can see that the order is less than we expect, with the aim of explaining what happens regarding the surface v_3, let us now take into account the surface v_2, exploiting the possibility of orienting the vector field $b(x, y)$ parallel to some of the curves of nondifferentiability of the surface. In particular, a very interesting result is presented in Table 4. In fact, starting with the images shown in Figure 13, we can see that the order is not close to 1 at all, but is almost 0.5. This depends on the vector field $b(x, y)$; in fact, from Figure 14

Table 3

Error in $L^\infty(\Omega_d)$ norm and order of convergence relative to v_3.

Δ	SL-F error	SL-F order	UW-F	UW-F order
0.02	1.890×10^{-1}		2.920×10^{-1}	
0.01	9.126×10^{-2}	1.050	2.064×10^{-1}	0.501
0.005	4.639×10^{-2}	0.976	1.339×10^{-1}	0.625
0.0025	2.905×10^{-2}	0.675	8.027×10^{-2}	0.738
Δ	SL-B error	SL-B order	UW-B	UW-B order
0.02	1.767×10^{-1}		1.781×10^{-1}	
0.01	1.119×10^{-1}	0.650	1.395×10^{-1}	0.353
0.005	7.564×10^{-2}	0.653	9.685×10^{-2}	0.526
0.0025	4.122×10^{-2}	0.775	6.145×10^{-2}	0.656

Table 4

Error in $L^\infty(\Omega_d)$ norm and order of convergence relative to v_2 with angles $\theta_1 = \pi$ and $\varphi_1 = 0.1$.

Δ	SL-F error	SL-F order	UW-F	UW-F order
0.02	6.221×10^{-2}		1.123×10^{-1}	
0.01	4.359×10^{-2}	0.5131	7.966×10^{-2}	0.493
0.005	3.068×10^{-2}	0.5067	5.638×10^{-2}	0.499
0.0025	2.164×10^{-2}	0.5036	3.989×10^{-2}	0.498
Δ	SL-B error	SL-B order	UW-B	UW-B order
0.02	6.221×10^{-2}		1.123×10^{-1}	
0.01	4.359×10^{-2}	0.5131	7.966×10^{-2}	0.493
0.005	3.068×10^{-2}	0.5067	5.638×10^{-2}	0.499
0.0025	3.989×10^{-2}	0.5036	3.989×10^{-2}	0.498

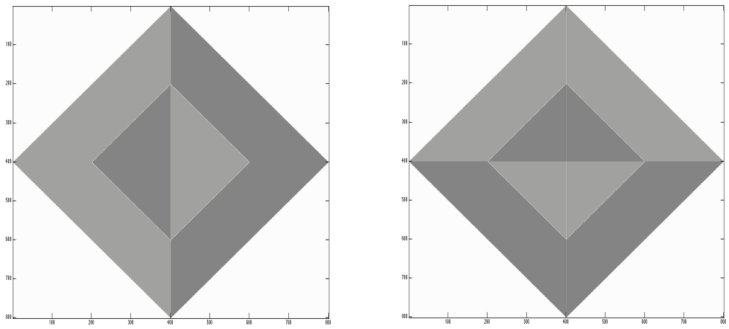

Test 4. I_1 for $\varphi_1 = 0.1$, $\theta_1 = \pi$. I_2 for $\varphi_2 = 0.1$, $\theta_2 = \frac{\pi}{2}$.

Figure 13. *The images that allow us to obtain a vector field $b(x, y)$ constant and parallel with respect to some curves of discontinuity of the surface.*

it is possible to see that some curves where the surface is not differentiable coincide exactly with the projection of the characteristics. For this kind of surface, even if the assumptions of Theorem 5.3 are satisfied, we have that the numerical schemes are convergent. The slower convergence order, in fact, depends on the coincidence of some discontinuous curve of the vector field $b(x, y)$ with the characteristic curves.

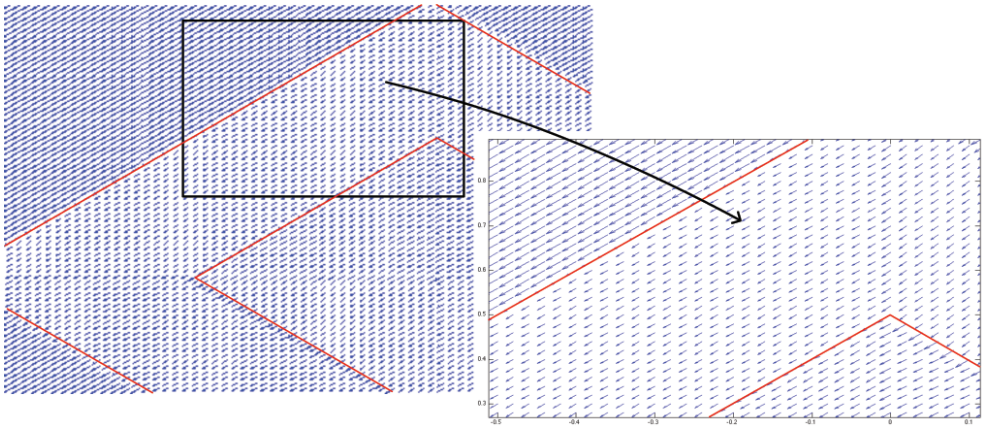

Figure 14. *In these overlapping images we emphasize in red the points where the surface is not differentiable. We also note that the vector field $b(x, y)$ (in blue) has the same direction as one of these curves.*

I_1 for $\omega' : \varphi_1 = 0.263, \theta_1 = -0.305$. I_2 for $\omega'' : \varphi_2 = 0.2, \theta_2 = 3.226$.

Figure 15. *Beethoven bust: real images.*

7.2. Real images. In this section we want to solve the SfS-PS problem in a real application. We apply it for the pictures of a Beethoven bust shown in Figure 15. The size of the images is 77×210 pixels, and the spherical coordinates of the light sources used for these pictures are written below each image.

The computing times relative to the semi-Lagrangian forward and backward schemes are, respectively, 2.033 and 2.13 seconds. The surfaces approximated with both schemes are shown in Figure 16.

Observing the computed surface, we note that the boundary condition is not satisfied on the right-hand side. This situation depends on the direction of the vector field $b(x, y)$ and on the error propagation in the numerical method. In fact, the propagation of the information

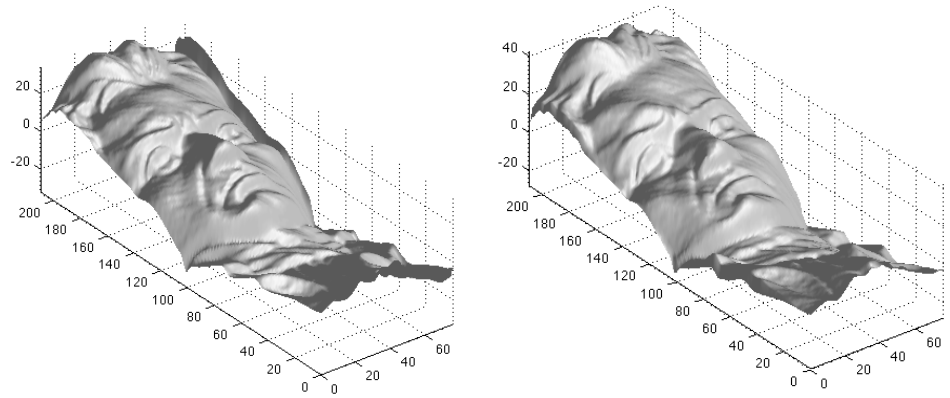

Figure 16. *Approximated surface of the Beethoven bust using the semi-Langrangian forward scheme (on the left) and the semi-Langrangian backward scheme (on the right).*

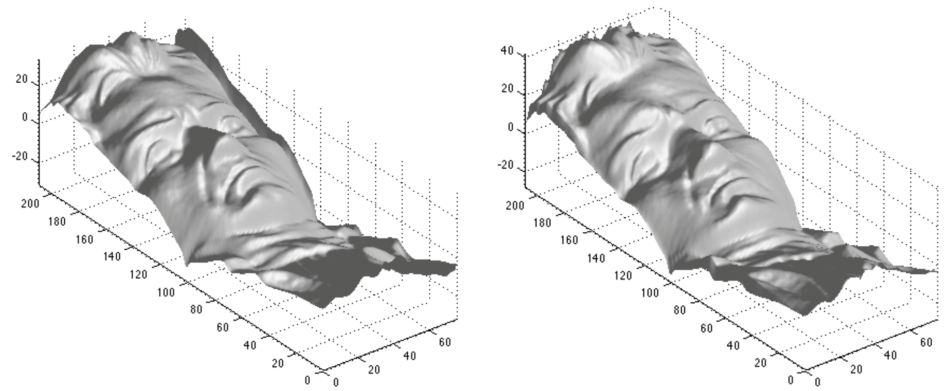

Figure 17. *Approximations of the Beethoven bust with the forward and backward upwind schemes, respectively, from the left to the right.*

is driven by $b(x, y)$, for the forward semi-Langrangian scheme starts from the left-hand side and arrives on the right-hand side accumulating errors. It is interesting to note that for the semi-Langrangian backward scheme, which starts from the right-hand side, the compensation of the errors during the iterations gives a better matching of the left boundary.

If we compute the surface using the upwind finite difference, we obtain the reconstruction of Figure 17. Clearly, considering that this numerical scheme follows the characteristics in the inflow direction, we obtain the same results as the semi-Langrangian forward scheme. The main advantage is related to the computing time. In fact, it needs only 0.12 seconds to converge. The same observations also can be done for the backward schemes.

From the left-hand pictures in Figures 16 and 17 (related to the forward approximation) it is possible to see that the reconstructed surface does not match with respect to the right side of the boundary condition. This is due to the fact that for this *direction* of reconstruction both numerical schemes do not need the boundary condition stored on the right boundary (i.e., on Γ_{out}). The reason they do not match is related to some real aspects which are not considered

in our assumptions, such as the not-so-exact orthographic view, the error on the light sources coordinates, and noise. They can bring a loss of consistency of the boundary condition (see section 5.1). Instead, for the backward schemes (shown in the right-hand pictures of Figures 16 and 17), even if they suffer from the same effects, a sort of compensation between them and the propagation error allows the matching between the surface and the left part of the boundary condition.

8. Conclusions and future perspectives. In this paper we have analyzed the SfS-PS problem under classical assumptions (introduced in section 2). We have shown that we can reduce the problem to a first order stationary linear PDE where the unknown is the surface $z = u(x, y)$, and we proved a uniqueness result in the class of Lipschitz continuous surfaces, provided that Dirichlet boundary conditions are given. The reconstruction of the real surfaces is based on the numerical solution of that linear PDE.

Two numerical methods have been proposed and analyzed: an upwind finite difference scheme and a semi-Lagrangian approximation scheme. Both converge, but the first is faster than and, in general, less accurate than the second. The fact that this approximation leads to good results in our tests in several benchmarks on virtual and real images motivates us to proceed with this research in new directions. The first direction is to consider an SfS model which includes perspective deformations as has been done for the classical problem with a single image. The second direction is to compare this method with a variational approach where the unknowns are $p = \partial u/\partial x$ and $q = \partial u/\partial y$, with the goal of reducing the demand for a priori knowledge of boundary conditions. We will develop these topics in our future work.

Appendix. Other numerical schemes. For the reader's convenience we will briefly describe the schemes corresponding to the integration of the characteristic field in opposite directions. These methods use the same construction as the schemes described in this paper, but they solve an equation with a reverse sign; i.e., they solve the following linear differential problem:

$$\text{(A.1)} \qquad \begin{cases} -b(x,y)\cdot\nabla u(x,y) = -f(x,y) & \text{a.e. } (x,y)\in\Omega, \\ u(x,y) = g(x,y) & \forall (x,y)\in\partial\Omega. \end{cases}$$

A.1. Backward semi-Lagrangian scheme. It is easy to check, using the same arguments presented in this paper, that the semi-Langrangian scheme for (A.1) is

$$\text{(A.2)} \qquad u_{i,j}^{n+1} = u^n(x_i + h\rho_1(x_i,y_j), y_j + h\rho_2(x_i,y_j)) - \frac{f_{i,j}}{|b_{i,j}|}h \quad \forall (x_i,y_j)\in\Omega_d,$$

where $\rho := b(x,y)/|b(x,y)|$. Note that now the vector field b has a reverse sign with respect to the forward scheme, so we will need the boundary conditions on the complementary part of $\partial\Omega$ used for the forward semi-Lagrangian scheme.

A.2. Backward upwind scheme. Using the same construction as the forward upwind scheme, we introduce an artificial diffusion that guarantees this time the possibility of following

the orientation of the characteristics in the other direction. The implicit numerical scheme

$$\begin{aligned}(\text{A.3}) \quad & -b^1_{i,j}\frac{U^B_{i+1,j}-U^B_{i-1,j}}{2\Delta}-b^2_{i,j}\frac{U^B_{i,j+1}-U^B_{i,j-1}}{2\Delta}\\ &\qquad =|b^1_{i,j}|\frac{U^B_{i+1,j}-2U^B_{i,j}+U^B_{i-1,j}}{2\Delta}+|b^2_{i,j}|\frac{U^B_{i,j+1}-2U^B_{i,j}+U^B_{i,j-1}}{2\Delta}-f_{i,j}\end{aligned}$$

for $i,j=1,\dots,n-1$ can be rewritten as

$$\begin{aligned}(\text{A.4}) \quad & U^B_{i+1,j}\left(\frac{b^1_{i,j}+|b^1_{i,j}|}{2\Delta}\right)-U^B_{i-1,j}\left(\frac{b^1_{i,j}-|b^1_{i,j}|}{2\Delta}\right)-U^B_{i,j}\left(\frac{|b^1_{i,j}|+|b^2_{i,j}|}{\Delta}\right)\\ &+U^B_{i,j+1}\left(\frac{b^2_{i,j}+|b^2_{i,j}|}{2\Delta}\right)-U^B_{i,j-1}\left(\frac{b^2_{i,j}-|b^2_{i,j}|}{2\Delta}\right)=f_{i,j},\end{aligned}$$

obtaining the block linear system with the same structure as the forward one. In particular in this case, denoting by D^B_r, $D^{S_B}_k$, $D^{I_B}_k$ (note that we used the upper index B to indicate that all the definitions refer to the backward scheme) the matrices of $\mathbb{R}^{(n-1)\times(n-1)}$, and by $U^B_{\text{bloc}_r}$, $b^B_{\text{bloc}_r}$ the vectors of $\mathbb{R}^{n-1}$ (with $r=1,\dots,n-1$ and $k=1,\dots,n-2$), we have that

$$D^B_r=\begin{pmatrix} -\frac{|b^1_{1,r}|+|b^2_{1,r}|}{\Delta} & \frac{b^1_{1,r}+|b^1_{1,r}|}{2\Delta} & 0 & \dots & \dots & 0\\ \frac{b^1_{2,r}+|b^1_{2,r}|}{2\Delta} & -\frac{|b^1_{2,r}|+|b^2_{2,r}|}{\Delta} & \frac{b^1_{2,r}+|b^1_{2,r}|}{2\Delta} & 0 & \dots & 0\\ 0 & \ddots & \ddots & \ddots & \ddots & 0\\ 0 & \dots & 0 & \frac{b^1_{n-2,r}+|b^1_{n-2,r}|}{2\Delta} & -\frac{|b^1_{n-2,r}|+|b^2_{n-2,r}|}{\Delta} & \frac{b^1_{n-2,r}+|b^1_{n-2,r}|}{2\Delta}\\ 0 & \dots & \dots & 0 & \frac{b^1_{n-1,r}+|b^1_{n-1,r}|}{2\Delta} & -\frac{|b^1_{n-1,r}|+|b^2_{n-1,r}|}{\Delta} \end{pmatrix},$$

$$D^{S_B}_k=\operatorname{diag}\left(\frac{b^2_{1,k}+|b^2_{1,k}|}{2\Delta},\frac{b^2_{2,k}+|b^2_{2,k}|}{2\Delta},\dots,\frac{b^2_{n-2,k}+|b^2_{n-2,k}|}{2\Delta},\frac{b^2_{n-1,k}+|b^2_{n-1,k}|}{2\Delta}\right),$$

$$\begin{aligned}D^{I_B}_k=\operatorname{diag}\Bigg(&-\frac{b^2_{1,k+1}-|b^2_{1,k+1}|}{2\Delta},-\frac{b^2_{2,k+1}-|b^2_{2,k+1}|}{2\Delta},\dots,\\ &-\frac{b^2_{n-2,k+1}-|b^2_{n-2,k+1}|}{2\Delta},-\frac{b^2_{n-1,k+1}-|b^2_{n-1,k+1}|}{2\Delta}\Bigg),\end{aligned}$$

$$B^B_{\text{bloc}_1}=\begin{pmatrix} u_{1,0}\frac{b^2_{1,1}-|b^2_{1,1}|}{2\Delta}+u_{0,1}\frac{b^1_{1,1}-|b^1_{1,1}|}{2\Delta}+f_{1,1}\\ u_{2,0}\frac{b^2_{2,1}-|b^2_{2,1}|}{2\Delta}+f_{2,1}\\ \vdots\\ u_{n-2,0}\frac{b^2_{n-2,1}-|b^2_{n-2,1}|}{2\Delta}+f_{n-2,1}\\ u_{n-1,0}\frac{b^2_{n-1,1}-|b^2_{n-1,1}|}{2\Delta}-u_{n,1}\frac{b^1_{n-1,1}+|b^1_{n-1,1}|}{2\Delta}+f_{n-1,1}\end{pmatrix},$$

$$B^B_{\mathrm{bloc}_q} = \begin{pmatrix} u_{0,q}\frac{b^1_{1,q}-|b^1_{1,q}|}{2\Delta} + f_{1,q} \\ f_{2,q} \\ \vdots \\ f_{n-2,q} \\ -u_{n,q}\frac{b^1_{n-1,q}+|b^1_{n-1,q}|}{2\Delta} + f_{n-1,q} \end{pmatrix} \qquad \text{for } q = 2, \dots, n-2,$$

$$B^B_{\mathrm{bloc}_{n-1}} = \begin{pmatrix} -u_{1,n}\frac{b^2_{1,n-1}+|b^2_{1,n-1}|}{2\Delta} + u_{0,n-1}\frac{b^1_{1,n-1}-|b^1_{1,n-1}|}{2\Delta} + f_{1,n-1} \\ -u_{2,n}\frac{b^2_{2,n-1}+|b^2_{2,n-1}|}{2\Delta} + f_{2,n-1} \\ \vdots \\ -u_{n-2,n}\frac{b^2_{n-2,n-1}+|b^2_{n-2,n-1}|}{2\Delta} + f_{n-2,n-1} \\ -u_{n-1,n}\frac{b^2_{n-1,n-1}+|b^2_{n-1,n-1}|}{2\Delta} - u_{n,n-1}\frac{b^1_{n-1,n-1}+|b^1_{n-1,n-1}|}{2\Delta} + f_{n-1,n-1} \end{pmatrix}.$$

REFERENCES

[1] S. M. Bakshi and Y. H. Yang, *Shape from shading for non-Lambertian surfaces*, in Proceedings of the IEEE International Conference on Image Processing, Vol. 2, IEEE Computer Society, Washington, DC, 1994, pp. 130–134.

[2] P. N. Belhumer, D. J. Kriegman, and A. L. Yuille, *The bas-relief ambiguity*, Int. J. Comput. Vision, 35 (1999), pp. 33–44.

[3] M. Breuss, E. Cristiani, J.-D. Durou, M. Falcone, and O. Vogel, *Numerical algorithms for perspective shape from shading*, Kybernetika, 46 (2010), pp. 207–225.

[4] M. Breuß, E. Cristiani, J.-D. Durou, M. Falcone, and O. Vogel, *Perspective shape from shading: Ambiguity analysis and numerical approximations*, SIAM J. Imaging Sci., 5 (2012), pp. 311–342.

[5] A. Chambolle, *A uniqueness result in the theory of stereo vision: Coupling shape from shading and binocular information allows unambiguous depth reconstruction*, Ann. Inst. H. Poincaré Anal. Non Linéaire, 11 (1994), pp. 1–16.

[6] W. Chojnacki, M. J. Brooks, and D. Gibbins, *Revisiting Pentland's estimator of light source direction*, J. Opt. Soc. Am. A, 11 (1994), pp. 118–124.

[7] F. Courteille, A. Crouzil, J.-D. Durou, and P. Gurdjos, *Towards shape from shading under realistic photographic conditions*, in Proceedings of the 17th International Conference on Pattern Recognition, IEEE Computer Society, Washington, DC, 2004, pp. 277–280.

[8] J. Van Diggelen, *A photometric investigation of the slopes and heights of the ranges of hills in the Maria of the Moon*, Bull. Astron. Inst. Netherlands, 11 (1951), pp. 283–290.

[9] M. S. Drew, *Direct solution of orientation-from-color problem using a modification of Pentland's light source direction estimator*, Comput. Vis. Image Underst., 64 (1996), pp. 286–299.

[10] J.-D. Durou, J.-F. Aujol, and F. Courteille, *Integrating the normal field of a surface in the presence of discontinuities*, in Proceedings of the 7th International Conference on Energy Minimization Methods in Computer Vision and Pattern Recognition, Springer-Verlag, Berlin, Heidelberg, 2009, pp. 261–273.

[11] J.-D. Durou and F. Courteille, *Integration of a normal field without boundary condition*, in Proceedings of the First International Workshop on Photometric Analysis for Computer Vision, PACV 2007, Rio de Janeiro, Brazil, 2007; available online at http://hal.inria.fr/inria-00264852/.

[12] J.-D. Durou, M. Falcone, and M. Sagona, *Numerical methods for shape-from-shading: A new survey with benchmarks*, Comput. Vis. Image Underst., 109 (2008), pp. 22–43.

[13] L. C. Evans, *Partial Differential Equations*, American Mathematical Society, Providence, RI, 2004.

[14] M. Falcone and R. Ferretti, *Semi-Lagrangian Approximation Schemes for Linear and Hamilton–Jacobi Equations*, SIAM, Philadelphia, to appear.
[15] D. A. Forsyth and A. Zisserman, *Reflections on shading*, IEEE Trans. Pattern Anal. Mach. Intell., 13 (1991), pp. 671–679.
[16] B. W. Hapke, *A theoretical photometric function for the lunar surface*, J. Geophys. Res., 68 (1963), pp. 4571–4586.
[17] J. K. Hasegawa and C. L. Tozzi, *Shape from shading with perspective projection and camera calibration*, Computers & Graphics, 20 (1996), pp. 351–364.
[18] B. K. P. Horn, *Shape from Shading: A Method for Obtaining the Shape of a Smooth Opaque Object from One View*, Ph.D. thesis, Department of Electrical Engineering and Computer Science, Massachusetts Institute of Technology, Cambridge, MA, 1970.
[19] B. K. P. Horn, *Obtaining shape from shading information*, in The Psychology of Computer Vision, P. H. Winston, ed., McGraw-Hill, New York, 1975, pp. 115–155.
[20] B. K. P. Horn and M. J. Brooks, *Shape from Shading*, The MIT Press, Cambridge, MA, 1989.
[21] S. Ishikawa, *Fixed points and iteration of a nonexpansive mapping in a Banach space*, Proc. Amer. Math. Soc., 59 (1976), pp. 65–71.
[22] R. Kozera, *Existence and uniqueness in photometric stereo*, Appl. Math. Comput., 44 (1991), pp. 1–103.
[23] K. M. Lee and C. C. J. Kuo, *Shape from shading with perspective projection*, CVGIP: Image Understanding, 59 (1994), pp. 202–212.
[24] K. M. Lee and C. C. J. Kuo, *Shape from shading with a generalized reflectance map model*, Comput. Vis. Image Underst., 67 (1997), pp. 143–160.
[25] S. Lee and M. Brady, *Integrating stereo and photometric stereo to monitor the development of glaucoma*, Image Vision Comput., 9 (1991), pp. 39–44.
[26] P. L. Lions, E. Rouy, and A. Tourin, *Shape-from-shading, viscosity solutions and edges*, Numer. Math., 64 (1993), pp. 323–353.
[27] R. Mecca and J.-D. Durou, *Unambiguous photometric stereo using two images*, in Proceedings of the 16th International Conference on Image Analysis and Processing, Part I, Springer-Verlag, Berlin, Heidelberg, 2011, pp. 286–295.
[28] R. Mecca and S. Tozza, *Shape reconstruction of symmetric surfaces using photometric stereo*, in Proceedings of the International Dagstuhl Seminar on Innovations for Shape Analysis: Models and Algorithms, Dagstuhl, Germany, 2011, Springer-Verlag, Berlin, Heidelberg, to appear.
[29] S. K. Nayar, K. Ikeuchi, and T. Kanade, *Shape from interreflections*, Int. J. Comput. Vision, 6 (1991), pp. 173–195.
[30] T. Okatani and K. Deguchi, *Shape reconstruction from an endoscope image by shape from shading technique for a point light source at the projection center*, Comput. Vis. Image Underst., 66 (1997), pp. 119–131.
[31] R. Onn and A. M. Bruckstein, *Integrability disambiguates surface recovery in two-image photometric stereo*, Int. J. Comput. Vision, 5 (1990), pp. 105–113.
[32] M. Oren and S. K. Nayar, *Generalization of the Lambertian model and implications for machine vision*, Int. J. Comput. Vision, 14 (1995), pp. 227–251.
[33] M. A. Penna, *A shape from shading analysis for a single perspective image of a polyhedron*, IEEE Trans. Pattern Anal. Mach. Intell., 11 (1989), pp. 545–554.
[34] E. Prados and O. Faugeras, *A Mathematical and Algorithmic Study of the Lambertian SFS Problem for Orthographic and Pinhole Cameras*, Technical report, Institut National de Recherche en Informatique et en Automatique, Sophia Antipolis, France, 2003.
[35] E. Prados and O. Faugeras, *"Perspective shape from shading" and viscosity solutions*, in Proceedings of the Ninth IEEE International Conference on Computer Vision, Vol. 2, IEEE Computer Society, Washington, DC, 2003, pp. 826–831.
[36] A. Quarteroni and A. Valli, *Numerical Approximation of Partial Differential Equations*, Springer-Verlag, Berlin, 1994.
[37] H. Rademacher, *Über partielle und totale Differenzierbarkeit von Funktionen mehrerer Variabeln und über die Transformation der Doppelintegrale*, Math. Ann., 79 (1919), pp. 340–359.
[38] H. Ragheb and E. R. Hancock, *A probabilistic framework for specular shape-from-shading*, Pattern Recognition, 36 (2003), pp. 407–427.

[39] T. Rindfleisch, *Photometric method for lunar topography*, Photometric Engineering, 32 (1966), pp. 262–277.

[40] E. Rouy, *Approximation numérique des solutions de viscosité des équations d'Hamilton-Jacobi et example*, Ph.D. thesis, Université Paris IX Dauphine, Paris, France, 1988.

[41] D. Samaras and D. N. Metaxas, *Coupled lighting direction and shape estimation from single images*, in Proceedings of the IEEE International Conference on Computer Vision, Vol. 2, IEEE Computer Society, Washington, DC, 1999, pp. 868–874.

[42] A. J. Stewart and M. S. Langer, *Toward accurate recovery of shape from shading under diffuse lighting*, IEEE Trans. Pattern Anal. Mach. Intell., 19 (1997), pp. 1020–1025.

[43] J. C. Strikwerda, *Finite Difference Schemes and Partial Differential Equations*, 2nd ed., SIAM, Philadelphia, 2004.

[44] A. Tankus and N. Kiryati, *Photometric stereo under perspective projection*, in Proceedings of the Tenth IEEE International Conference on Computer Vision, IEEE Computer Society, Washington, DC, 2005, pp. 611–616.

[45] A. Tankus, N. A. Sochen, and Y. Yeshurun, *A new perspective [on] shape-from-shading*, in Proceedings of the Ninth IEEE International Conference on Computer Vision, IEEE Computer Society, Washington, DC, 2003, pp. 862–869.

[46] G. Ulich, *Provably convergent methods for the linear and nonlinear shape from shading problem*, J. Math. Imaging Vision, 9 (1998), pp. 69–82.

[47] Y. Wang and D. Samaras, *Estimation of multiple illuminants from a single image of arbitrary known geometry*, in Proceedings of the Seventh European Conference on Computer Vision, III, Springer-Verlag, London, 2002, pp. 272–288.

[48] T. Wei and R. Klette, *A New Algorithm for Gradient Field Integration*, Communication and Information Technology Research Technical Report 103, Computer Science Department, University of Auckland, Auckland, New Zealand, 2001.

[49] R. Zhang, P. S. Tsai, J. E. Cryer, and M. Shah, *Shape-from-shading: A survey*, IEEE Trans. Pattern Anal. Mach. Intell., 21 (1999), pp. 690–706.